



Università di Pisa

---

DIPARTIMENTO DI FISICA "ENRICO FERMI"

Corso di Laurea in Fisica

TESI DI LAUREA

## Commissioning and first data analysis of the Mainz radius experiment.

Candidato:

**Adriano Del Vincio**

Matricola 562946

Relatore:

**Prof. Francesco Forti**

**Prof.ssa Concettina Sfienti**

# Contents

<b>1 Physics motivation for neutron skin thickness measurement.</b>	<b>6</b>
1.1 Nuclear equation of state (EOS) and neutron skin thickness. . . . .	6
1.2 Parity-violating scattering experiment . . . . .	6
1.3 Transverse asymmetry . . . . .	6
1.3.1 Motivation . . . . .	6
1.3.2 Conventions used . . . . .	6
<b>2 Transverse Asymmetry</b>	<b>7</b>
2.1 Description of the process . . . . .	7
2.1.1 Elastic scattering . . . . .	9
2.1.2 Inelastic scattering . . . . .	9
2.1.3 Model description . . . . .	9
2.2 State of the Experiment . . . . .	9
<b>3 Experimental setup.</b>	<b>11</b>
3.1 Overview of the experiment. . . . .	11
3.2 Mami . . . . .	12
3.2.1 Acceleration stage. . . . .	12
3.2.2 Polarized Beam. . . . .	12
3.2.3 Polarization measurement. . . . .	13
3.2.4 Moller and Compton polarimeters . . . . .	14
3.3 Experimental hall setup. . . . .	14
3.4 Detectors and beam monitors . . . . .	15
3.4.1 Detectors A and B . . . . .	15
3.4.2 Beam monitors. . . . .	17
3.4.3 Beam stabilization. . . . .	19
3.5 Electronics . . . . .	19
3.5.1 VFCs . . . . .	19
3.5.2 Nino board . . . . .	19
3.5.3 Master Board . . . . .	20
<b>4 Detectors Test, alignment and calibrations.</b>	<b>21</b>
4.1 Data tree implementation . . . . .	21
4.2 Detectors test . . . . .	22
4.3 Calibrations. . . . .	26
4.3.1 Alignment of the scattering plane. . . . .	26
4.3.2 Calibration of the VFCs monitors. . . . .	26
4.3.3 Beam monitors calibration. . . . .	27
4.3.4 Current (PIMO) and energy monitors (ENMO) calibration. . . . .	29
4.3.5 Calibration of the PMTs . . . . .	31
4.3.6 Autocalibration procedure . . . . .	33
<b>5 Asymmetry on Carbon and Rates on Lead target.</b>	<b>37</b>
5.1 Rates on lead . . . . .	37
5.2 Model for fitting the data . . . . .	38
5.3 Data pre-selection and Fit . . . . .	39
5.3.1 Fit with a linear model . . . . .	44
5.4 False asymmetries . . . . .	47
5.5 ??Bootstrap?? . . . . .	49

<b>6 Result</b>	<b>50</b>
6.1 Best fit . . . . .	50
<b>7 Conclusion and outlook</b>	<b>53</b>
<b>Appendices</b>	<b>54</b>
<b>A Some Appendix</b>	<b>55</b>

# Commissioning and first data analysis of the Mainz Radius Experiment.

Adriano del Vincio

## Abstract

The Mainz Radius Experiment (MREX) is an experimental campaign with the aim of determining fundamental properties of the equation of state (EOS) of nuclear matter. The equation of state is the fundamental quantity that contains all the thermodynamic properties of a system of nucleons and describes the relation between energy, pressure, temperature, density and asymmetry between the number of neutron and the number of proton in nuclear-matter. An important parameter, poorly-known at the state of current knowledge, is the slope of the symmetry energy at saturation density  $L$ , which quantifies the dependencies of the energy per nucleon associated with the changes in neutron-proton asymmetry. This key component controls how the energy of a system of nucleons change whether there is a difference in the number of proton and neutrons and it is also an underlying contribution to the determination of neutron stars radius whose physical description, despite being many order of magnitude higher than the physical dimensions of the nuclei, is still determined by the EOS, too. The slope of the symmetry energy  $L$  is strongly correlated to a characteristic shown by heavy nuclei, the neutron-skin thickness, that is the difference between the spacial distribution radius  $R$  of the neutrons and protons. Nowadays it is well-known from various nuclear physics experiments that the neutrons of a nucleus tends to locate more externally, forming a neutral thin layer around atomic nuclei. This peculiar characteristic shown by heavy nuclei is known in literature as neutron-skin thickness. The experimental measurement of this quantity is the main method to estimate the value of  $L$ , which is used as an input of many existing theoretical models of neutron stars. The MREX is focused on the determination of the neutron skin thickness of  $^{208}Pb$  from parity-violating experiments (PV) performed at the future MESA electron accelerator, that is currently under construction and will be located in Mainz. The parity-violating experiments, where longitudinal polarized electrons scatter from a fixed target at a single value of momentum transfer, consist on the determination of the asymmetry  $A_p$  in the number of scattered electrons due to the different longitudinal polarization of the beam, and are valid probe to determine the neutron-skin thickness of heavy-nuclei. In this context, it is necessary to determine one of the possible background sources for the PV experiments, known as beam normal single spin asymmetry, or transverse asymmetry, which consists in a small transverse electron polarization component which produce an effect that is of the same order of magnitude of the  $A_{pv}$ . The transverse asymmetry  $A_n$  comes from the interference between the diagrams in which one or two virtual photons are exchanged, their contribution is on the order of 20 ppm part-per-million. The work of this thesis focuses on the measurement of the transverse asymmetry  $A_n$  carried out at the Mainz microtron accelerator (MAMI) on a  $^{12}C$  target. The  $^{12}C$  target is particularly suited for studying and testing the electronic systems and detectors that will be employed in the next phase of the MREX experiment, the determination of  $A_n$  for  $^{208}Pb$ . The measure consist in the determination of  $A_n$  using two detectors made of two cherenkov fused-silica materials coupled to 3 and 8 photo-multipliers tubes. The two detectors have been tested in the laboratory, together with the new electronic for the data read-out, that consist in the NINO-asic board with which the impulse signals coming from the detectors are acquired. The data collected during the beam-time have been analyzed developing a new analysis program, which in summary take care of processing the raw-data to compute the beam parameters that are relevant for the analysis. The beam parameters, as the  $X$ ,  $Y$  position of the beam (with  $Z$  parallel to the beam direction),  $\theta_x$  and  $\theta_y$  scattering angles, and the  $I,E$  current intensity and energy are determined with particular accuracy because their variation over time can result in effects that overlap with  $A_n$ . The analysis deals with separating the contributions of these false asymmetries from  $A_n$ . The work of analysis consisted in a first part dedicated to the calibration of the monitors, to measure the parameters of the beam, and the two detectors. The second part was focused in the analysis of the data collected during the beam time, removing the outliers and identifying and possible errors and isolating the contribution of false asymmetries.  $A_n$  has been measured for  $e^-$ - $^{12}C$  scattering at a two fixed angles ( $\theta_B = -22.5^\circ$ ,  $\theta_A = 22.5^\circ$ ) corresponding to a transfer momentum of  $Q^2 = 0.04$  GeV. The measured values are:  $A_B = -22 \pm 5$  (stat) ppm (part per million) for detector B and  $22.8 \pm 1.7$  (stat) ppm for detector A. The different sign of the two measures is in agreement with the opposite kinematic, and the two measure are compatible within  $1\sigma$ , and in agreement with the previous measurement performed at MAMI.

# Organization of Contents

the work-flow of my thesis can be summarized in a first part (corresponding to chapter 1 and chapter 2) which describes in details the underlying physics and the motivation for the measurement of the PV scattering and  $A_n$ , and a second part focused on the hardware work and data-analysis which is summarized in the following step:

- Description of MAMI experimental setup and beam characteristics. Explanation of beam measurement equipment and the interface with the electronics developed for the MREX experiment.
- Description and characterization of the detectors with test in the laboratory.
- Electronic tests and characterization.
- Development of the analysis program, check of the program with simple monte-carlo simulation together with specific unit test.
- Description of the calibration phase, data pre-selection and removal of the outliers.
- Data-analysis for  $^{12}C$  and extraction of the  $A_n$ . Raw estimation of the systematic effects of the measurement and determination of the rates with the lead target, in prevision of the future experiment with  $^{208}Pb$ .

The result obtained are discussed and compared with the other measurements performed by different collaborations. Finally the confront with the theoretical prediction discussed in chapter 2 is done.

# Chapter 1

## Physics motivation for neutron skin thickness measurement.

- 1.1 Nuclear equation of state (EOS) and neutron skin thickness.
- 1.2 Parity-violating scattering experiment
- 1.3 Transverse asymmetry
  - 1.3.1 Motivation
  - 1.3.2 Conventions used

# Chapter 2

## Transverse Asymmetry

**introduction** This chapter is focused on describing the theory behind the transverse asymmetry. The transverse asymmetry arises from interference between two scattering amplitudes and it is deeply connected with the Time-reversal operator. These two contributions due to the electromagnetic interaction between the incident electron and the nucleus are explained by showing what are the limits of current theory and what are the most important terms in theoretical prediction. The chapter ends by presenting the problem of the anomalous observation made by PREX of zero transverse asymmetry and a study on the accuracy with which it is possible to measure the asymmetry.

### 2.1 Description of the process

The Beam Normal single spin asymmetry, which we will refer for brevity as Transverse asymmetry, originates from the interference of two scattering process. For the purpose of this thesis, we will present the case of electron scattering against a spin 0 target [4]. To understand why the interference of this two scattering amplitude give rise to an asymmetry, we first have to look at the kinematic of the experiment:

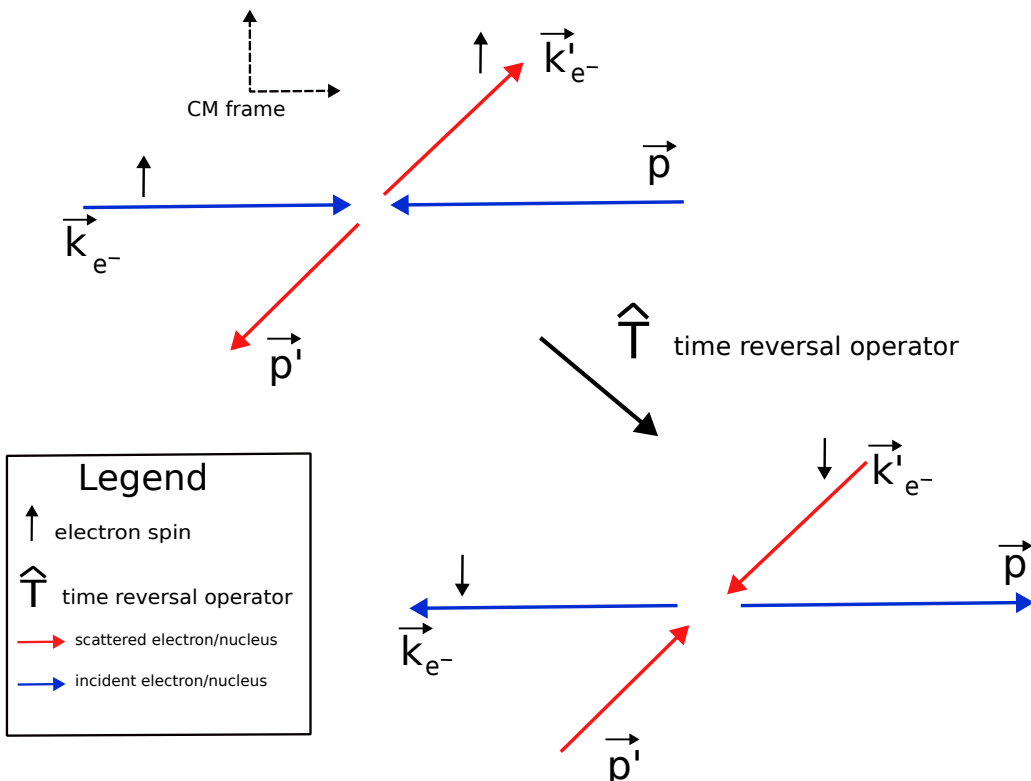


Figure 2.1: Scheme of the scattering process. In blue the incident electron and nucleus, in red the outgoing electron and nucleus. All the quantities are referred to the center of mass frame. The small arrow over the vector represent the electron spin, aligned in the normal plane.

Where all the momenta are measured respect to the center of mass frame. In the figure we can confront

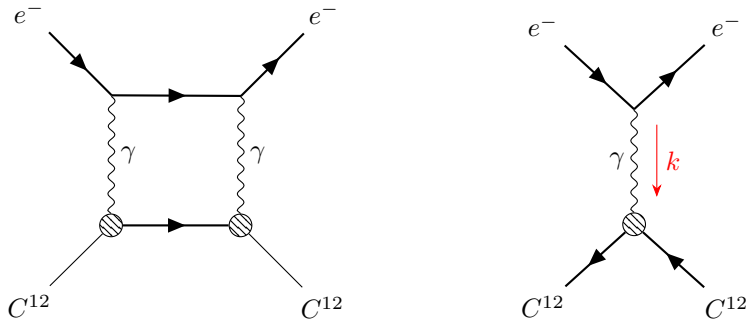


Figure 2.2: TPE and OPE diagrams in electron nucleus scattering.

the two situation before and after applying the Time-reversal operator,  $\hat{\Theta}$ . Looking at the picture we can understand that :

- Before applying  $\hat{\Theta}$ , we have the incident electron with  $\vec{k}$  momenta and the nucleus with  $\vec{P}$  momenta, after applying  $\hat{\Theta}$  we have that the incident/outgoing electron and the incident/outgoing nucleus are exchanged.
- The  $\hat{\Theta}$  operator acts also on the spin of the electron. Because we are considering process where the spin doesn't flip, the two situations are not equivalent.
- Considering that the process is elastic, the kinematic is the same, taking  $\vec{p}$  and  $\vec{k}$  as the initial particle momenta, or  $\vec{p}'$  and  $\vec{k}'$ .

The time-reversal operator seems to connect the two different cases of UP and DOWN polarized electron. Our effort is to measure the asymmetry between the two cross section:

$$A = \frac{\sigma_{\uparrow} - \sigma_{\downarrow}}{\sigma_{\uparrow} + \sigma_{\downarrow}} \quad (2.1)$$

And it's particularly clear that a non-zero asymmetry depends on how the time-reversal act on the elastic amplitude of the process.

With this idea, let's see in more detail the  $\hat{\Theta}$ . We know that  $\hat{\Theta}$  is an antiunitary operator that can be always seen as:

$$\hat{\Theta} = U \cdot K$$

Where  $U$  is an unitary operator, while  $K$  is the complex conjugation operator that generates the complex conjugate of each coefficient in front of it. If we consider a ket describing a system we have that:

$$Kc|\alpha\rangle = c^*K|\alpha\rangle \quad (2.2)$$

Now, let's consider  $H$  as the hamiltonian of our system. We want to apply the  $\hat{\Theta}$  operator. We can now use the assumption that the hamiltonian consist of two term, which correspond to the two different scattering process. Because of the electromagnetic interaction conserve  $CP$ , so also  $T$  is conserved, we know in advance that each piece of the hamiltonian commute with  $\hat{\Theta}$ . Now let's see what happen for an hamiltonian which has an imaginary part:

$$H = H_R + iH_{Im} \quad ; \quad \hat{\Theta}H\hat{\Theta}^{-1} = \hat{\Theta}H_R\hat{\Theta}^{-1} + \hat{\Theta}iH_{Im}\hat{\Theta}^{-1} \Rightarrow H_R - iH_{Im} \neq H \quad (2.3)$$

what we understand from these simple calculation is that to give rise to an asymmetry, we expect an imaginary part of the scattering amplitude different from zero.

At the  $\alpha$  leading order, the two process of the electron-Nucleus scattering that give rise to the asymmetry involve the exchange of one-photon-exchange (OPE) and two-photon-exchange (TPE). The Feynman diagrams that describes the processes are the following:

A seguire come si scrive l'ampiezza per il termine elastico ed inelastico, aggiungere in appendice come viene fatto l'integrale sullo spazio delle fasi e stop.

### 2.1.1 Elastic scattering

### 2.1.2 Inelastic scattering

### 2.1.3 Model description

$$A_N = C_0 \cdot \log\left(\frac{Q^2}{m_e^2 c^2}\right) \frac{F_{Compton}(Q^2)}{F_{ch}(Q^2)} \quad (2.4)$$

## 2.2 State of the Experiment

We have seen so far how the Transverse Asymmetry is related to the interference between two scattering amplitude, and the theoretical model used to describe the process. The goal from an experimental point of view is to measure this quantity. The challenge is to obtain a valid measure of  $A_n$ , which is of the order of 20 part per million (ppm), taking into consideration all the possible effects that can interfere. To measure  $A_n$ , the straightforward method is to prepare an electron beam, with polarized electron, and send it to a fixed target. The scattered electrons are then collected by a detector placed at a certain angle, and now it's possible to obtain the transverse asymmetry applying the formula:

$$A(Q, p) = \frac{N_\uparrow(Q) - N_\downarrow(Q)}{N_\uparrow(Q) + N_\downarrow(Q)} \cdot \left(\frac{1}{p}\right) \quad (2.5)$$

where we have explained the dependence on the transmitted impulse, on the degree of polarization of the beam. In an experiment of this type, several requests are necessary to have an effective data acquisition:

- The accelerator must produce a polarized beam, stable over the time, with an high polarization percentage, in order to amplify the effect.
- The Beam energy needs to be quite stable, and should not depend on the Polarization state of the electrons. A change in the Beam energy associated with the polarization state, can lead to a different count rate for  $N_\uparrow$  and  $N_\downarrow$ , would make a contribution that would be added to that of the physical process
- The beam must be correctly aligned with the target, and stable. Again if the position of the target changes according to the polarization of the electrons, it will produce another contribution to the total asymmetry.
- The beam current should not depend on the polarization state of the electrons. If the beam source depends on the polarization, we will have a difference in the event rate and then another false asymmetry.
- it's necessary to reject possible double elastic scattering events, which may contribute to the total asymmetry.

All this demands can be satisfied with an accelerator that has stabilization devices with great precision and that can sustain high beam intensities. This last request is necessary to accumulate enough statistics to measure the transverse asymmetry with an accuracy about 1 ppm, in view of the future PV experiments. We can quantify how the statistical error varies according to the amount of data available. With the quite general assumption that the measured rate  $N_{\uparrow, \downarrow}$  are gaussian distributed variables, we can compute the expected variance of  $A_n$ :

$$Var[A_n] = \frac{1 - A^2}{N_\uparrow + N_\downarrow} \quad (2.6)$$

This is the variance associated to a single measurement of the transverse asymmetry. As is well known, the variance scales as  $\frac{1}{n}$  as  $n$ , the number of measures, increases. Because the  $A_n$  is expected to be quite small, we can approximate the above formula:

$$V[A_n] = \frac{1}{2N \cdot n} \quad (2.7)$$

The error associated to the reconstructed asymmetry is the square root of the above quantity. If we impose that the error must be  $\leq 1\text{ppm}$  we can easily obtain that the quantity  $n \cdot N$ :

$$n \cdot N \leq \frac{1}{2} \cdot 10^{12}$$

We will see later that achievable rates  $N_{\uparrow,\downarrow}$  are in the range (20000,100000) for a carbon target. This number can not be increased at will by acting on the beam current. The first reason is obvious: the accelerator and the beam source can handle only a certain amount of electrons before losing their characteristics, furthermore a beam with great intensity for an extended periods of time can damage the carbon target, up to the risk of melting it. Another idea might be to increase the thickness of the target, to take advantage of the larger cross section. However this does not take into account that by doing so the number of double scattering event is increased. To avoid this the scientific community that deals with these nuclear physics measurements respect the convention that the target thickness should be less than the 10% of the radiation length of the material.

# Chapter 3

## Experimental setup.

**introduction** This chapter presents briefly the structure and the characteristics of the Mainz microtron accelerator (MAMI), where the transverse asymmetryasymmetry is measured, and the experimental setup used. Particular attention is shown in the the description of the beam monitors, that are quite specific for the standard of particle accelerators. Following an overview of MAMI and the acceleration stages, the experimental hall and the specific electronics devices to acquire and process the data are presented.

### 3.1 Overview of the experiment.

To measure the Beam-Normal single spin asymmetry, a polarized beam of 570 MeV will be sent against a 10 mm width of  $^{12}C$  target. The detectors consist of two fused-silica coupled to 3 (detector B) and 8 (detector A) pmts, which collect the Cherenkov light emitted when an electron pass through the fused-silica. The detector are placed inside the two spectrometer of the A1 hall, which are not used in this experiment due to the high luminosity of the beam ( $20 \mu\text{A}$ ) that is above their limits of operation. The asymmetry due the change of the electrons spin is the aim of the measurement. The pmts signals are collected and digitalized by the **NINO** board, after a threshold selection, and sent to the A1 control room computer, where the DAQ program collect the data together with all the data coming from the Beam monitors producing Binary files, which are later analyzed by the analysis program, which is significant part of the work done in the framework of the thesis. The data collected are divided in *Events* made by 4 *sub-events* in sequence. Each event correspond to a temporal window of  $\simeq 80 \mu\text{s}$ , where each sub-event is  $20 \mu\text{s}$  long. Here it's important to clarify that unlike the majority of experiments in high energy physics, an event is made by all the electrons interacting with the detectors during the time interval of the event, and we will refer to this hereafter unless otherwise stated. The division into sub-events reflects the polarization sequence of the beam. The PMTs counts and the beam monitor values are saved for each sub-event, along with the time length of the event (measured by in clock cycle by the NINO electronic board 3.5.2), and other values which are required to process beam monitor data.

The general structure of the event is the following:

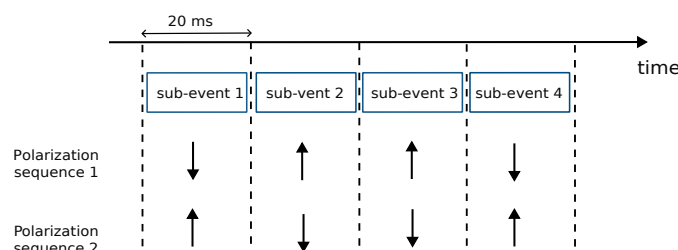


Figure 3.1: Event structure

The two polarity pattern are selected randomly using a De Bruijng sequence, (**spiegare cosa è e come è implementata**). For each event we have a single measure of  $A_n$ , defined ad the asymmetry between the  $\uparrow$  adn  $\downarrow$  sub-events.

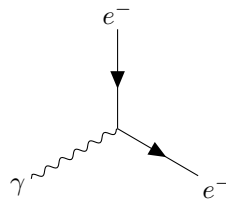
## 3.2 Mami

### 3.2.1 Acceleration stage.

### 3.2.2 Polarized Beam.

For the beam-normal single spin asymmetry a vertical polarized beam is necessary. At the MAMI electron accelerator is possible to produce a vertical polarized beam with energy in the range 180 MeV – 855 MeV [5]. In this section the procedure to orient the beam vertically is presented, following an explanation of how the degree of polarization of the beam is measured.

The electron source used at MAMI is made by a strained GaAs/GaAsP superlattice photocathode illuminated by circular polarized light. A Pockels cell changes the helicity of the photons impinging on the electrons. The extracted electron has the same helicity of the incoming photon, let's suppose as an example:



$$(Jz)_\gamma = \pm 1 \quad (Jz)_{e^-} = \mp \frac{1}{2} \rightarrow \pm \frac{1}{2} \quad (3.1)$$

With the fast change of the Pockels cell it is possible to alternately revert the sign of the polarization. By the insertion of a  $\lambda/2$  plate between the laser system and the photo-cathode the polarization orientation of the electron beam can be reversed for each sub-event, useful later for the estimation of systematic errors. The beam polarization achieved with this source is roughly 80%, for the beam time it was : 0.79%

To switch from longitudinal polarization to transverse polarization, two devices are used: the **Wien filter** and a **double solenoid** located in the injection beam line.

*bird's eye view*

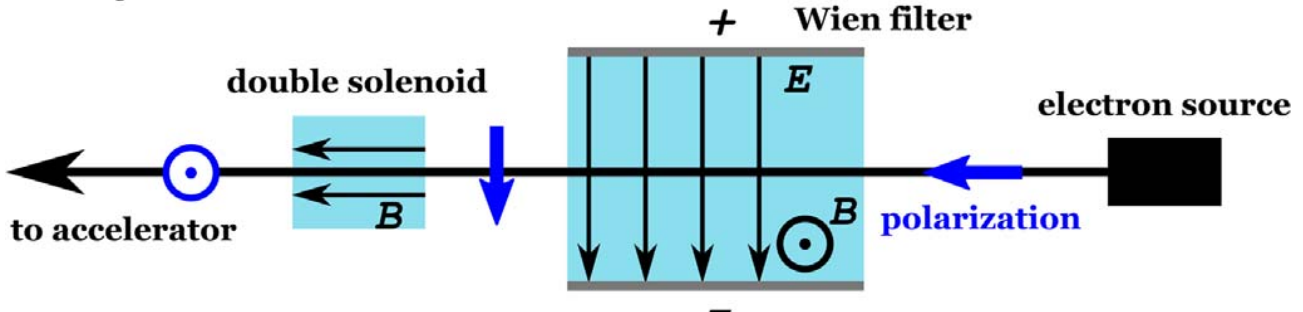


Figure 3.2: Setup for the transverse polarization.

Following the picture, the spin of the electrons from the source are rotated first in the XY plane with a  $90^\circ$  rotation, then the subsequent double solenoid align the spin to the vertical direction with another  $90^\circ$  rotation. Once the beam pass the double solenoid, the electrons go through linac, the microtron and in the end to the experimental hall, where the target of the experiments is installed. During the acceleration stage, the spins follow the precession motion due to the various magnetic fields of the accelerator; the equation that determine how the spin precession for relativistic electrons is the BMT equation. However, the magnetic field of the various bending magnets, for example the magnets of the microtron, is always parallel to the vertical direction, and to the electrons polarization, too; so only the residual horizontal component precedes during the motion. For conventional experiment that involve a longitudinal polarization, after the first spin rotation, there is a further rotation due to the motion in the accelerator. Because of this, the rotation made by the Wien is set in such a way that after the second rotation due to the motion in the accelerator, the polarization has the correct alignment in the experimental hall. The rotation angles of the polarization vector through the accelerator are known from simulations and are also directly measured for relevant energies, for a beam of 570 MeV the rotation angle is  $55^\circ$  with an accuracy of  $\pm 2^\circ$ . In our case, this further rotation has only a small effect to the residual horizontal component, whose effect is negligible compared to the  $A_n$  that we want to measure.

At the beginning MAMI was not developed for experiment with transverse polarization. So it's not possible to measure directly the transverse component. However combining the measurement in the XY plane, with

the existing setup, it is possible to get the polarization value also in that direction. For this purpose a Moller, Compton and Mott polarimeters are used.

### 3.2.3 Polarization measurement.

**Briefly explain how the Mott polarimeter works, for measuring the polarization of the beam.**

To Measure the polarization of an electron beam different polarimeters can be used. Here we explain briefly the physics underlying the *Mott* polarimeter, used in the experiment. Consider an electron beam that is sent towards a nucleus of charge  $Ze$ . We know from theory that the spin of the incident electron is affected by the electromagnetic field produced by the nucleus. This can be described calculation the magnetic field seen by a particle with speed  $\vec{v}$  near a nucleus:

$$\vec{B}_{nucleus} = \frac{-\vec{v} \times \vec{E}_{nucleus}}{c} = \frac{Ze}{mc^2 r^3} \vec{L}$$

$$V = -\mu \cdot \vec{B}_{nucleus} = \frac{Ze}{mc^2 r^3} \vec{L} \cdot \vec{S}_{e^-}$$

The second equation represent the spin-orbit interaction potential. This term yields the polarization dependence of the cross section, and it is exploited to obtain the polarization of the incident particles. Indeed the cross section can be model highlighting the dependencies on the spin  $\vec{S}$ :

$$\sigma(\theta) = I(\theta)[1 + S(\theta)\vec{P} \cdot \vec{n}]$$

Let's consider an incident particle that scatter from a nucleus at an angle  $\theta$ , as shown in the figure:

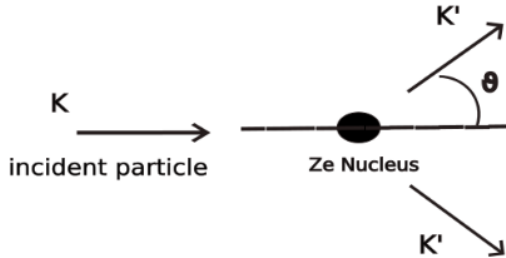


Figure 3.3: Scheme of the Mott scattering, the polarization is orthogonal to the plane,  $\vec{n} = \frac{\vec{k} \times \vec{k}'}{|\vec{k} \times \vec{k}'|}$

The direction of  $\vec{n}$  depends on whether scattering to the left or right is being considered. Let's suppose our initial beam has a polarization  $P$ , and so we compute the asymmetry  $A(\theta)$  of the scattered electrons between left ( $N_L$ ) and right ( $N_R$ ).  $N_L$  and right  $N_R$  will be proportional respectively:

$$N_L = N_{\downarrow}[1 + S(\theta)] + N_{\uparrow}[1 - S(\theta)]$$

$$N_R = N_{\uparrow}[1 + S(\theta)] + N_{\downarrow}[1 - S(\theta)]$$

$$A(\theta) = \frac{N_L - N_R}{N_L + N_R} = \frac{N_{\downarrow}(1 + S(\theta)) + N_{\uparrow}(1 - S(\theta)) - N_{\uparrow}(1 + S(\theta)) + N_{\downarrow}(1 - S(\theta))}{N_L + N_R} = \dots = P \cdot S(\theta)$$

From the last equation we have a relation which give the beam polarization in terms of  $A(\theta)$  (which is what is measured) and the asymmetry function  $S(\theta)$  (known also as Sherman function). There are several calculation of the Sherman function, which is well-known for high energy electron scattering.

The total beam polarization is measured by a Moller polarimeter, in the experimental hall, with the beam polarization oriented longitudinally in the experimental hall. The Moller polarimeter can measure the longitudinal polarization of the beam. The other two polarimeters, Compton and Mott, located behind the injector linear accelerator (ILAC), are sensitive to the longitudinal and the trasverse horizontal components of the beam (with an energy around 3,5 MeV at this stage). The procedure for the allignment is the following: at the beginning of the beam time the Mott polarimeter is used for different settings of the solenoidal field, with the Wien filter angle equal (nominal) to  $90^\circ$ . The aim is to minimize the horizontal polarization component after the rotation performed by the double solenoid, changing the solenoidal magnetic field. Then a second optimization follows, using the Moller polarimeter for different Wien filter angles is performed. With the new Wien filter settings, another measurement is performed with the Mott polarimeter.

### 3.2.4 Moller and Compton polarimeters

## 3.3 Experimental hall setup.

Until now we have described how MAMI produce and accelerate the electrons, however we do not presented the structure where the beam is delivered and various experiments are carried out.

MAMI has 3 different hall, named with the capital letter A followed with a number, which indicate also the different collaboration that work with the experiments. In A2, as an example, photo-nuclear reactions are studied to investigate the fundamental physics at the scale of nuclear dimensions. The experimental hall where the experiment treated described in this thesis is conducted is the A1 hall. We will describe briefly the main operating detectors that are installed and the details that are interesting for the transverse asymmetry measurement.

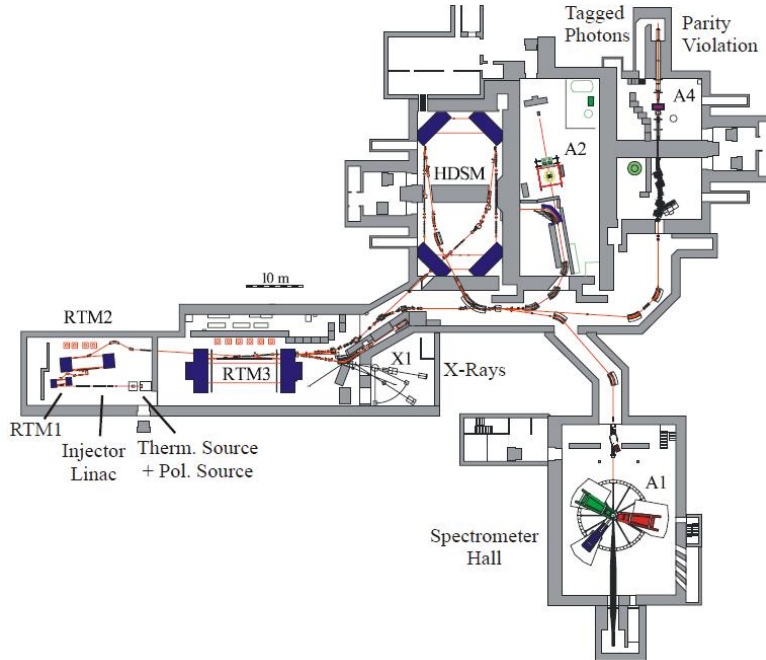


Figure 3.4: Scheme of the accelerator, with the different experimental hall. Actually the A4 hall is restructured, in fact it will host the future Mesa accelerator.

In A1, experiment with fixed target are conducted. The electrons can be delivered with an energy up to 1,6 GeV, after passing the last acceleration stage (HDSM, in the figure). Because the electron energy of our experiment is 570 MeV, the beam will pass through the first acceleration steps, the linac (linear accelerator) and Race-track system and when the desired energy is achieved the electrons will be sent to the A1 experimental hall.

Inside A1 hall three large magnetic spectrometers are placed on a circular rail-track the target chamber. These spectrometers were designed and built in 1993 to perform high precision measurement of electron scattering in coincidence with other hadron detection, with a high resolution in the determination of the particle momenta  $\frac{\delta p}{p} < 10^{-4}$ . The spectrometers develop vertically with a height of 15 m, for this reason the scattered electrons and the other particles are deflected with the use of the magnetic field respect to the scattering plane. The following figure shows the path the particle scattered from the target:

The spectrometers used for the transverse asymmetry are the ones shown in the picture. There are multiple reasons why the particle are deflected on the vertical direction, we summarized them in two points:

- reason of space, due to the fact the an horizontal setup would not fit with the dimension of the building in addition to the fact that this would not allow to rotate the spectrometers by a variety of angles that the vertical orientation does
- reduce background and noise, in fact the high beam intensity that is possible to reach at MAMI is a source of noise and background event which can be cut off detecting the particle far from the interaction point.

Once a particle is scattered in the acceptance region of the detectors, the magnetic field deflect the particle that passes through a drift chamber, which occupies the first third in height of the spectrometers. When the particle is at the height of the platform in the figure, it impinge on a layer of plastic scintillator, and after that

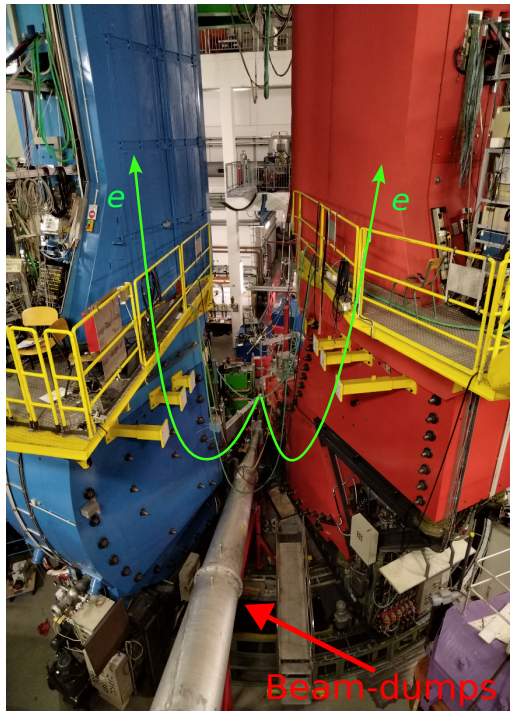


Figure 3.5: Image of the spectrometers of A1 hall. The spectrometers can be rotated using a system of railtracks that are visible at the bottom of image. The electrons are scattered and then deflected in the vertical direction by the magnetic field (green lines). This picture is taken from behind the target, so we see the beam-dumps. The target is roughly at the center of the image where the two green lines join. The electron are coming on the opposite direction, respect to the spectrometers.

a Cherenkov detector which measures the particle speed  $\vec{v}$ . We have a picture of the spectrometers internal, taken during the installation of the two detectors (that will be presented in the next section) 3.6.

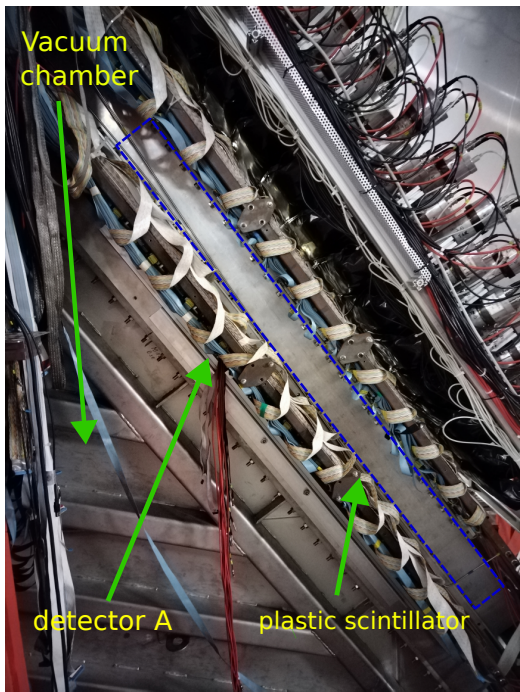


Figure 3.6: Internal of the A spectrometer. This image was taken during the installation of the detector A inside the red spectrometer, that is accessible from the platform visible in the other picture : 3.5

The determination of both the particle speed  $\vec{v}$  and momenta (drift chamber) allows to identify the particles. Despite the possibilities offered by the already existing setup, for the beam time of interest none of these components was used directly in the estimation of  $A_n$ . The reason is due to the high intensity of the beam that is used in the experiment, which is far from the optimal operating conditions of the components, that are suited for rates lower than the ones expected for beam normal single spin measurements. The spectrometers then will be used indirectly for the alignment of scattered electron to

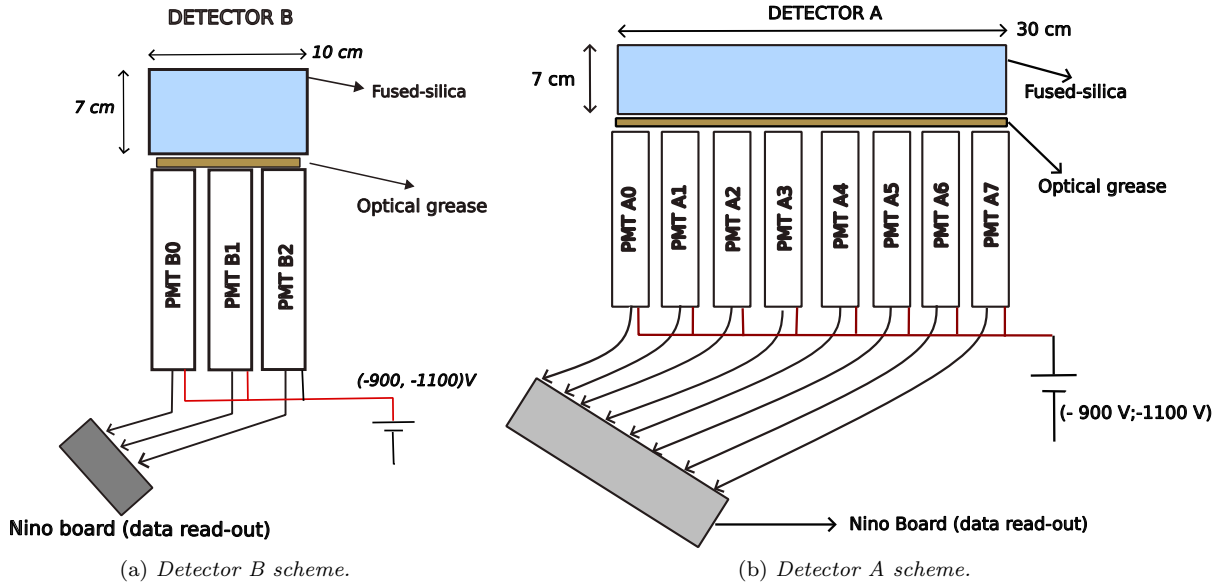
## 3.4 Detectors and beam monitors

### 3.4.1 Detectors A and B

In this section we will describe the electronics and the detectors used to measure the transverse asymmetry. For this experiment we are going to measure the transverse asymmetry at different angles. The electrons detection is made via two thin blocks of fused-silica that are coupled to PMTs. When a scattered electron hit the fused-silica (refractive index  $n = 1.45$ ) Cherenkov light is emitted. The emitted cherenkov light can interact with the electrons of the material, which, in turn, can hit the PMT dyode. This sequence of event triggers the PMT and produce an output signal.

In the experiment, we will measure the transverse asymmetry at two angles of scattering, so two detectors are installed and read-out independently. The two detector are made by 3 PMTs and 8 PMTs coupled with two blocks of fused-silica, a scheme of the detector is shown below:

These two detectors are placed inside the spectrometers presented in , between the top of the drift-chamber, which occupies the first third in height of the spectrometer, and just below a



panel of scintillator. During the beam time the drift chamber of the spektrometers is turn off, and also the PMTs coupled to the spektrometer scintillators are not powered.

As we mention above, the scattered electron are deflected in the vertical direction by the magnetic field of the spektrometer. At this moment, it is important to mention the differences between the new and the old electronic setup. In the old electronic setup the output signal of the PMTs was integrated during the time interval of each sub-event, and therefore the single scattered electron could not be counted. The advantage of this method is that the electronics is more simple, in fact there in no need to develop a fast counter, unlike the new setup, where the new electronic take into account of every pulses. However, this old method is effected by a baseline noise and it's not good for the future experiments with lead target, where the expected rates are lower than the rates on carbon. With the new electronics, all the single electron are counted, and this will allow the future measurements with lead, improving the accuracy.

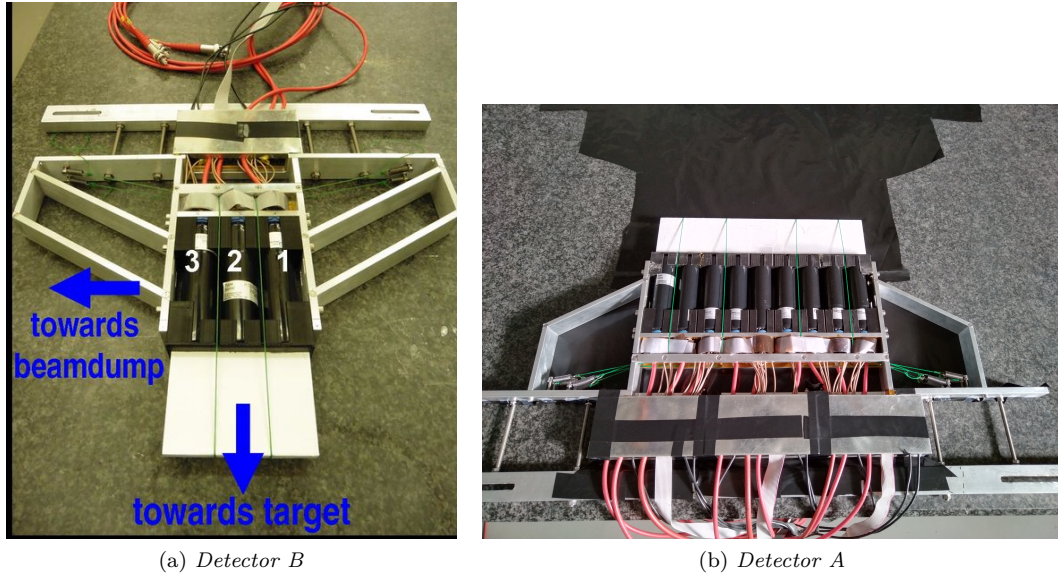


Figure 3.7: Picture of the two detector taken in the clean room. The white blocks are the fused silica that produces the Cherenkov light, the cylinders below are the PMTs.

Here we report the characteristic of the two detector that are relevant for the data analysis:

- detector B size (length, height, depth):  $7\text{ cm} \times 10\text{ cm} \times 1\text{ cm}$
- detector A size (length, height, depth):  $7\text{ cm} \times 30\text{ cm} \times 1\text{ cm}$
- Number of dynodes: .

- The Power voltage for the PMT in negative, in the range of  $(-900 \text{ V}, -1100 \text{ V})$
- refraction index  $n$  of the fused-silica is 1.45.

### 3.4.2 Beam monitors.

In MAMI, several monitors are placed along the beam line in order to check beam quality and measure parameters such as current intensity, energy and relative position of the beam. This section summarize an explanation of the operating principles of the monitors installed at MAMI. The explanation will be partial, some details will be given in the appendix, however for a complete discussion please refer to the following paper ([2]).

The monitors available at MAMI are quite specific for the standard of the particle accelerators. Resonant cavities are used to measure the various quantities, with the underlying physical principle that the passage of charged particles through these cavities can excite some electromagnetic resonant modes<sup>1</sup> which can be detected and analyzed by an analogic circuit to measure the beam parameters. Before going into the details, is necessary to define some quantities that will be used later in the explanation. We define  $r_s$ , the Shunt-impedance as :

$$r_s = \frac{|V_{\parallel}|^2}{P} \quad (3.2)$$

$P$  is the power absorbed by the cavity when a particle excites one of the resonant mode, instead  $V_{\parallel}$  is defined as the effective voltage surpassed by a charged particle along a straight line, which can be computed as:

$$V_{\parallel} = \frac{1}{q} \int_{s_0}^{s^1} \vec{E}_s \vec{e}_s ds$$

The Shunt impedance is a measure of the interaction strength between a cavity and a charged particle, and can be expressed also in another way, introducing the  $Q$  value of the cavity,  $W$  the maximum energy stored and  $f_r$  the frequency of resonance:

$$r_s = \frac{|V_{\parallel}|^2 Q}{2\pi f_r W}$$

When the beam travel through the cavity, the particles release energy that excites the oscillation mode. The power  $P_{HF}$  extracted from the beam is related to the beam current:

$$P = i^2 r_s$$

An antenna is used to decouple part of the energy from the cavity and send it to a circuit which produces an analog output signal. Indicating with  $\kappa$  the coupling constant of the antenna, the previous relation need to be modified introducing a new factor  $\frac{\kappa}{(1+\kappa)^2}$ . In a Cylindrical resonator, the same type installed at MAMI, the resonance frequency of the different oscillation modes is expressed by the formula

$$f_{m,n,p} = \frac{c}{2\pi\sqrt{\epsilon_r\mu_r}} \sqrt{\left(\frac{x_{m,n}}{R}\right)^2 + \left(\frac{p\pi}{L}\right)^2}$$

The constants in the formula are:

- $c$  is the light speed.
- $\epsilon_r, \mu_r$  are the magnetic and dielectric constant of the material.
- $x_{m,n}$  is the n-th zero of the m-th Bessel function.
- $R$  and  $L$  are the radius of the cylindrical cavity and its length.
- 

---

<sup>1</sup>TM mode, where the magnetic field is completely transverse respect to particle momenta

This formula can be obtained solving the Maxwell equations with cylindrical boundary condition, the eigenvalues are the given by the formula above.

If the frequency of the Beam bunch is equal to the resonant frequency  $f_{m,n,p}$  of the cavity, a TM mode is excited. At MAMI high quality monitors are installed, quantitatively all the monitors have a  $Q \simeq 10000$ , that means that  $\frac{\nu}{\delta\nu} \simeq 10000$ . This means that the frequency of the beam bunch must be very close to the frequency of the resonant cavity. At MAMI the frequency used for all the resonators is 2,449 532 GHz or a multiple of it. The beam bunch frequency is the same, and it's controlled by the MAMI-master oscillation signal, that is the reference signal for all the MAMI monitors.

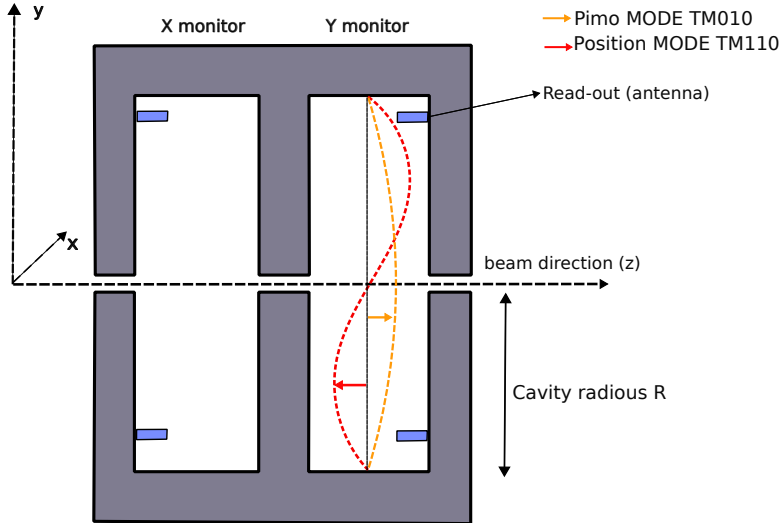


Figure 3.8: Scheme of the Cylindrical cavities installed at MAMI. In red we have the  $TM_{110}$  mode, used to measure the position of the beam, in yellow the  $TM_{010}$  mode, to measure the intensity of the beam.

Depending on the  $TM$  mode excited, we have a different signal in the cavity, so a different signal collected by the antenna. The relevant quantity that is detected is the power  $P_{HF}$  absorbed by the antenna. For the  $TM_{010}$  mode, the power is

$$P_{HF} = i^2 r_{010} \frac{\kappa}{(1 + \kappa)^2} \quad (3.3)$$

The power absorbed by the antenna is directly dependent on the beam current. Because the rage values are typically in the range of pW to mW, the signal is processed in close proximity of the installed monitors. In the signal process, the input signal of the antenna is coupled to the master-oscillation signal, so the output signal is given by the formula:

$$U = \sqrt{P_{HF}} \cos(\phi - \phi_{LO}) \quad (3.4)$$

the phase  $\phi$  is the phase of the resonant mode or the phase of the beam bunch, while the phase  $\phi_{LO}$  is the phase respect to the master-oscillation signal, and can be adjusted by a phase shifter of the circuit. The output voltage signal can be read out with the oscilloscope or digitalized and saved with other devices. To measure the beam intensity is important to minimize  $\phi - \phi_{LO}$ , to maximixe the signal amplitude, and then the output signal is ready to be analyzed.

The measurement of the  $x, y$  position follows in principle the same procedure. In this case the  $TM_{110}$  is acquired. The reason is clear, because it's possible to calculate that for this mode the  $r_{shunt}$  is proportional to the beam position on the  $x, y$  plane. So The power absorbed by the antenna can be written:

$$P_{HF} = i^2 r_{110} \frac{\kappa}{(1 + \kappa)^2} Kx^2 \quad (3.5)$$

with the output signal prortional to the square root of the absorbed power, we end with:

$$x, y = \sqrt{(P_{HF})} = costant \cdot \frac{U}{i} \quad (3.6)$$

With this is clear how it's possible to measure all the important quantity related to the beam that will be used for the analysis.

### 3.4.3 Beam stabilization.

## 3.5 Electronics

### 3.5.1 VFCs

Some parameters which describe the beam are needed in order to take into account possible effect in the measure of the Transverse asymmetry. The relevant data are the position in the  $(x, y)$  plane, the incident angles on the target, the current and energy of the beam. All this values are collected using the already existing monitors. To collect the data from the monitors, single and multichannel, synchronous voltage-to-frequency converters (AD7742) are used. This devices contain an analog modulator that is able to convert the input voltage into an output pulse train, whose frequency is proportional to the input voltage.

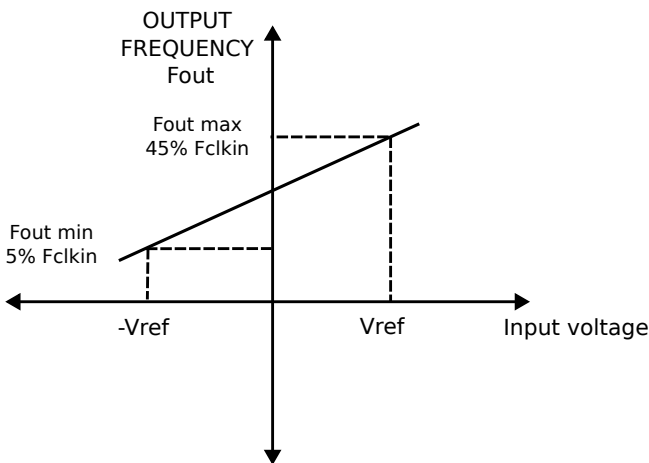


Figure 3.9: Frequency versus Voltage

The VFCs are powered with an external tension of 5 V, and a differential voltage input in the range  $(-V_{ref}, V_{ref})$  is also applied. An external clock signal, that is indicated with "CLKIN" is provided as a reference signal for the oscillator frequency. The analog input signal is sampled with by a switched capacitor, with a rate that is controlled by clock that can be supplied externally, in our case we used a 6 MHz. A scheme of the electronic circuit is drawn here (*aggiungere figura*), the output of the Comparator is a fixed width pulse (the pulse is initiated by the edge of the clock signal) with a frequency that goes from  $0.5\% \cdot f_{CLKIN}$  to  $0.45\% \cdot f_{CLKIN}$  [1], where the first correspond to 0,0 V in input and the second to  $V_{ref}$ . Neglecting possible systematic errors, the relation the output frequency and the input voltage is the following:

$$V_{in} = \frac{V_{ref}}{40\% \cdot f_{CLKIN}} (f_{out} - 5\% f_{CLKIN}) \quad (3.7)$$

We control the  $f_{CLKIN}$  with the period of the clock. The data are acquired counting the number of pulses that come from the comparator, so we can substitute to  $f$  the number of pulses (the two quantities are proportional), and we end with:

$$V_{in} = V_{ref} [2 \cdot \frac{N_{pulses} - 5\% N_{CLKIN}}{40\% N_{CLKIN}} - 1] \quad (3.8)$$

### 3.5.2 Nino board

The NINO board is our data acquisition system for the PMT counts. It is made by 32 analog input channels and it is powered with  $\pm 5$  V. Each channel has an attenuator, and the signal pass through that before going to the Comparator, which compare the signal to the threshold. The Output signal is a Low-voltage differential signaling (LVDS). Each comparator can handle eight channel and for each of them it is possible to define a global threshold. With the current settings of NINO board, it is possible to change the threshold of each channel acting on another value, the attenuation, which decreases the value of the global threshold. All the value that can be modified are 12 bit numbers, so a setting interval of  $(0.; 4095)$ . The NINO board is designed in such

a way that collects the Input charge of the signal, operating with a 30 pF. The output signal amplitude is proportional to the input charge, and it is sent to the discriminator. Our interest is only to count the number of scattered electron, so we do not intend to measure the input charge, but only a signal is produced or not.

Two Nino board are used in the experiment, one for detector A and one for detector B. For the experiment discussed in this thesis, we will use only 8 channel for detector A and 3 channel for detector B, since this is the number of the input signals coming from the two detectors. For the future experiments more channel will be used, splitting the analog input signal in 4 different signal, sending it to 4 different input channel of the board. This is useful because changing individually the attenuation value, we can define 4 different thresholds for the same signal coming from a single PMT. This is something useful to compare different values of threshold, for example to study how the noise affect the measurement, and see what is the right compromise between signal and noise . The way we selected the threshold is explained in the following chapter (Analysis).



Figure 3.10: Nino Board

### 3.5.3 Master Board

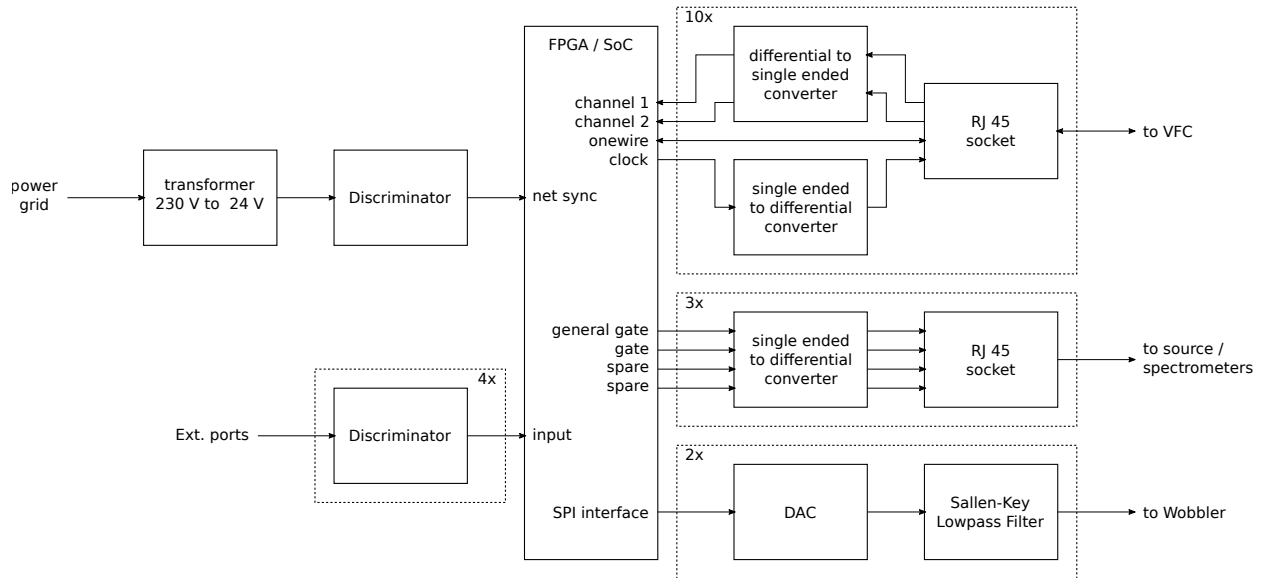


Figure 3.11: Scheme of the master-board, the device that coordinates all the electronics for the experiments, and send the data to the computer in the control room.

# Chapter 4

## Detectors Test, alignment and calibrations.

**Introduction** In this chapter we discuss the electronic test that have been carried out in the laboratory, and the calibrations that need to be done in order to calculate, from the raw data, the final data ready for the analysis. The test in the lab consist in checking that the photo-multipliers are working and that the electronics that take care of acquiring the data do not have any errors. For the calibrations, since several beam parameters are needed for the analysis, it's important to obtain the correct scaling factor to convert the Raw Data collected by the *VFCs* to data with the right physical units. The important quantities are the  $X, Y$  impact point coordinates of the beam, the energy  $E$ , the beam current  $I$  and the scattering angles  $\theta_x$  and  $\theta_y$ .

### 4.1 Data tree implementation

Referring to the next picture, we now discuss briefly the structure of the data that is implemented in the analysis program, this is important to clarify how data analysis will be developed:

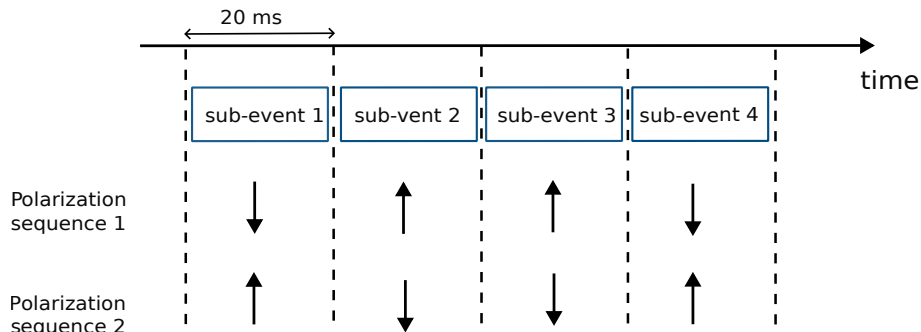


Figure 4.1

The base class that is implemented in the analysis program is the *Event* class. As we mention above in 3.1, we do not intend to keep track of the single scattered electron, instead we analyze time series of 80 ms, in which we simply count all the electrons detected in this time interval. The work-flow of the analysis program is load the binary file collected during the beam time, parsing one event at a time and processing the raw-data from the beam monitors and the detectors. During the execution of the program data files in *.txt* are generated and filled with the processed data ready. The output data-file can be analyzed with any software package, such as root or python, to get the value of the asymmetry  $A_n$ . The picture shows that every event is divided into 4 sub-events. For each different sub-event a precise state of the polarization is defined, +1 for  $S = \uparrow$  and -1 for  $S = \downarrow$ . Every sub-event is 20 ms long; during this time interval master-board receives all the data coming from the monitors and the detectors and sent them to the data-acquisition program (DAQ) that produces the binary-files, which are the input of the main analysis program.

It is important to note that for each sub-event, a single measurement is acquired from the beam monitors, which is intended as a time average of the various signals on the 20 milliseconds of sub-event duration. The sampling rate is then equal to 50 Hz.

This structure of the data is quite specific for particle physics experiment. The main reason for this setup is connected with the need to avoid as much as possible that the variations of intensity, position and energy of

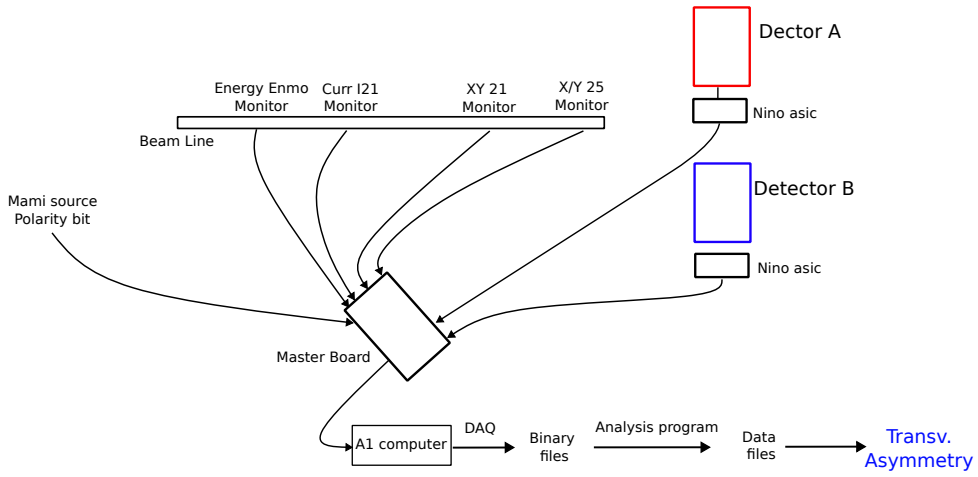


Figure 4.2: Scheme of the data flow.

the beams induce an effect that add to  $A_n$ . Considering only small time series, it is assumed that the beam is quite stable, in order to reduce undesired effects. Nevertheless, the contribution of these effects, which are indicated for brevity as false asymmetries, is considered in the final model. Several values are saved with the number of scattered electrons, for each event. Here we will present briefly all the various quantities that are saved, and the general structure of the data tree:

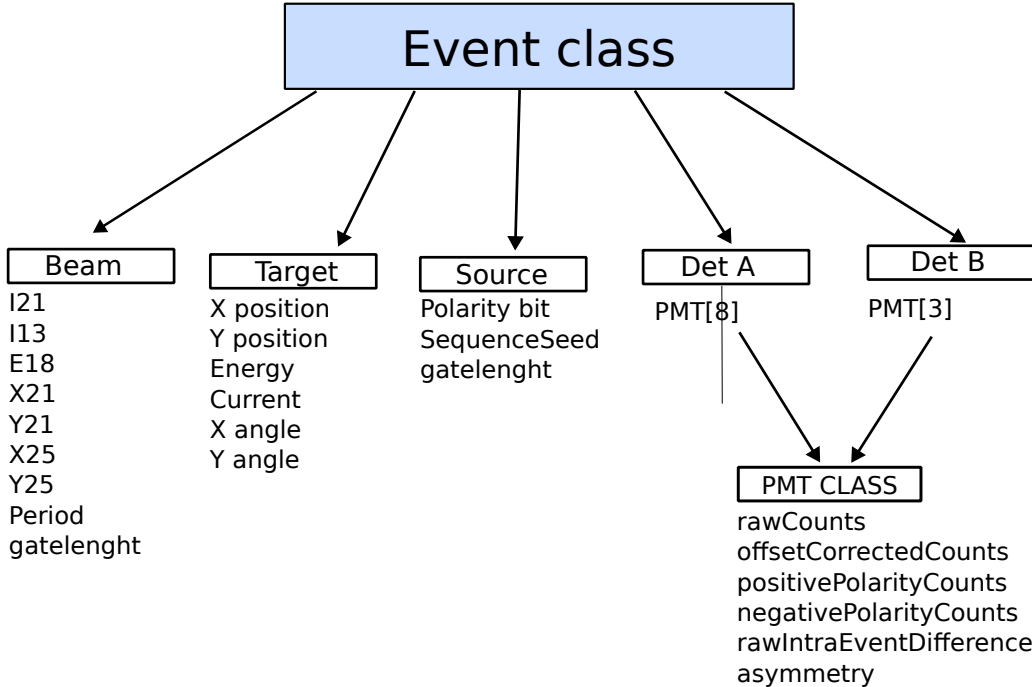


Figure 4.3: Scheme of the Event class, the structure of the data tree is shown here in a simplified version, for the complete reference see appendix.

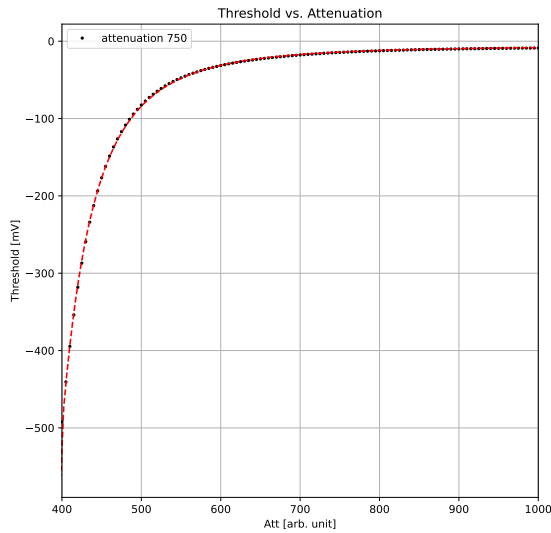
## 4.2 Nino Board threshold selection

In this section we explain briefly simple test that we performed to control that the two detectors are working properly. Before going into detail it is important to describe again the operation of the NINO board, which interfaces directly with detectors. The Nino board, which digitizes the signal from the PMTS, has two parameters which can be used to select the internal threshold of the discriminator, to cut out the low amplitude signals, that are indicated as threshold and attenuation. The threshold and attenuation values can be adjusted changing the settings of the DAQ program. For our purpose, we fix the threshold values equal to 600 for all the detectors. We remind the reader that the values should be in the range (0, 4000). It is desirable to work with the "physical" values, i.e switch from these arbitrary units to the correct value in mV. The relation between

attenuation and threshold it is not linear, the reason is that the NINO board is designed in such a way that collects the input charge coming from the signal. In principle it is even not possible to define a unique value for the threshold in mV, because signals that produce the same charge can have shape and amplitude different from each other. In simple word, from the definition of the current:

$$Q = I \cdot time \quad (4.1)$$

Signal with a large time width and a small amplitude can generate the same accumulation of charge respect to narrow signal with high voltage amplitude. Despite this, some data have been acquired by the A1 collaboration, with which it's possible to define a raw conversion function from attenuation units to threshold. The basic idea is to fix the time-length and the shape of signal and vary the amplitude, then we can observe the minimum value of attenuation for which the NINO board collects the input signal. We are aware that for electrons that hit the detectors, the shape of the signal could be different, and are not fixed, however this procedure let us to have at least a first rough estimate of the threshold value.



(a) *Threshold dependence against attenuation*

The data show represent the values of the amplitude of the input signals (in m) versus attenuation, the function used for the conversion is obtained from the fit of the data, the function used is the following:

$$Threshold = \frac{a}{(att - b)^3} + c \quad (4.2)$$

The values obtained from the fit are:

- $a = -802111053 \frac{\text{mV}}{\text{arb. unit}}$
- $b = 382 \text{ [arb. unit]}$
- $c = -6,1 \text{ mV}$

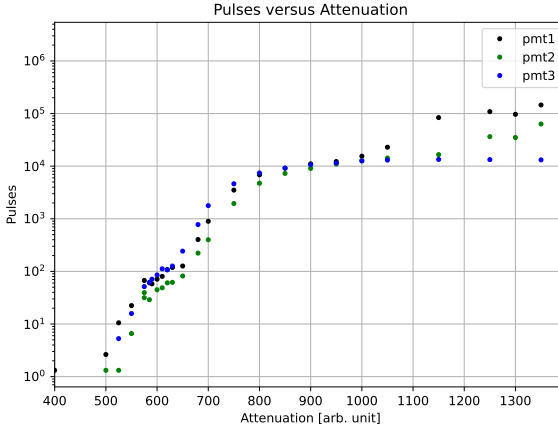
### 4.3 Detectors test

Before the Beam time, some test with the two detectors were performed, to check that the pmts were still working after some years of inactivity, and that the new electronic was able to count properly the pulses and store the data. For this studies, we didn't have a radioactive sources to employ, so we moved the two detectors in the workshop of the accelerator, and we use the cosmic rays rate as a probe.

Knowing that the expected number of event for cosmic rays is about  $1 \frac{\text{event}}{\text{cm}^2 \text{s}}$  we can compute the expected values for the number of events. We decided to take 1 minute long acquisition for both the two detectors, this leads to 70 expected events for detector B and 100 events for detector A.

The first step is to select a good point of work for the threshold. So, fixing the value of the threshold parameter for the NINO board, we took several acquisitions, each of them one minute long, increasing each

time the attenuation. We powered the pmts with a negative voltage around  $-1000\text{ V}$ , as suggested in the data-sheets, and covered the cherenkov detector with a shielding blanket, to avoid ambient light simulating a signal.



(a) Attenuation scan for Detector B

We observed a small knee in the plot, around the zone of  $580 - 600$  of attenuation, where the number of counts was almost constant, roughly equal to the number of expected events from muons hitting the detector. Then we observe a big edge for attenuation = 1000. Looking at the plot 4.4a, we assume that the attenuation values are so high that electronic noise is no longer rejected, in fact the counts grow enormously. The attenuation was set at 600.

The next step was to study the statistical fluctuation of the counts, so we collected 10 acquisitions, each of them 1 min long. The measured values are reported in the table below:

Pmt:	1	2	3
1	58	60	62
2	62	55	59
3	61	59	70
4	73	66	70
5	68	66	56
6	59	52	64
7	69	74	77
8	48	49	57
9	70	54	58
10	60	61	66

This data are interesting to check if the counts are following the theoretical distribution of the events expected for cosmic rays at sea level. If the pmt are working in a good mode, we know that the number of counts should be Poisson-distributed:

$$Pdf(\mu, k) = \frac{\mu^k}{k!} e^{-\mu} \quad (4.3)$$

The variance of the Poisson distribution is equal to the mean of the counts, and we expect the same behaviour also for the sample mean and the sample variance:

$$\begin{aligned} \mu_1 &= 62.8 & \sigma_1^2 &= 54.40 & r_{12} &= 0.66 \\ \mu_2 &= 59.6 & \sigma_2^2 &= 57.15 & r_{23} &= 0.65 \\ \mu_3 &= 63.9 & \sigma_3^2 &= 46.98 & r_{13} &= 0.35 \end{aligned}$$

We report also the correlation  $r_{xy}$  between the pmt. The result are fine: we are able to see a positive correlation between adjacent pmt, and as expected the correlation is lower in the case of the more distant. This is explained by the lower probability that the photons of Cherenkov radiation light up at the same time pmts that are far away from each other. We can test that the data follow a Poisson distribution using the well-known Gosset test, defined as:

$$\chi_{n-1}^2 = \sum_{i=1}^n \frac{(Oss_i - Att_i)^2}{Att_i} \quad (4.4)$$

We report the result obtained with the data for detector B, the test shows that there is good agreement with the hypothesis that the count are Poisson-distributed.

Pmt:	1	2	3
$\chi^2_9$	8.52	8.45	6.37

To convince oneself that the pmt are actually measuring signals given by the passage of cosmic rays, and not only noise, we placed one pmt in coincidence with the others. If we are able to observe positive correlation between the counts, we conclude that the signal comes from the same event.

pmt	0	1	2	4 (in coincidence)
1	63	57	72	28
2	55	51	64	18
3	62	53	75	27
4	71	62	75	33
5	68	59	49	23
6	57	55	63	18
7	70	64	64	24
8	50	69	69	25
9	65	62	62	19
10	74	71	77	28

As above, we report the sample mean, the variance and the correlation between the pmt in coincidence and the detector B:

$$\begin{aligned} \mu_0 &= 63.5 & \sigma^2 &= 58.9 & r_{04} &= 0.49 \\ \mu_1 &= 60.3 & \sigma^2 &= 43.3 & r_{14} &= 0.38 \\ \mu_2 &= 67.0 & \sigma^2 &= 71.1 & r_{24} &= 0.65 \end{aligned}$$

The pmt number 4, that is the pmt in coincidence with the detector, was placed geometrically over the pmt number 2. We observe a positive correlation for the values  $r_{04}, r_{14}, r_{24}$ , the correlation is higher for the pmt number 2, and less for 0 and 1, for a geometrical reason.

Pmt:	1	2	3	pmt in coincidence
$\chi^2_9$	8.95	6.44	10.96	9.52

The same procedure was followed also for detector A. We analyzed 4 signal at a time, because during these lab test we had only one NINO board, with only 4 channels available.

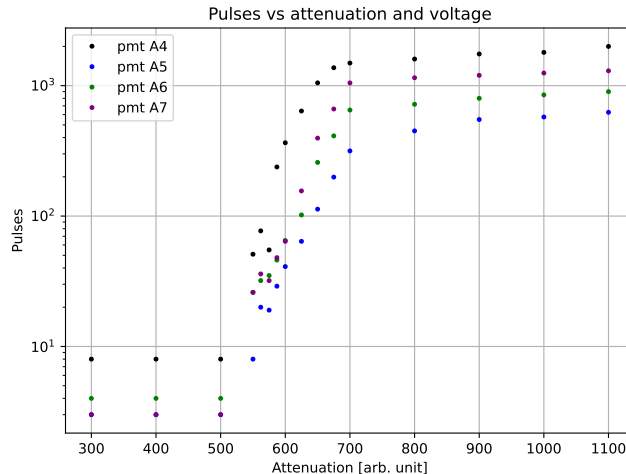


Figure 4.4: Attenuation scan for Detector A, for the pmt 4-5-6-7

We repeat the same test of detector B also for this 4 pmts, without finding any problem or strange behavior. The same procedure was repeated also for the last 3 Pmts of detector A, we took as above 10 acquisitions 1 minute long to study the count distribution, with one pmt in coincidence:

pmt	2	1	0	(in coincidence)
1	91	51	50	27
2	86	61	50	7
3	58	48	45	18
4	95	62	41	29
5	69	60	50	21
6	85	57	45	19
7	66	51	46	28
8	74	51	48	22
9	77	43	45	17
10	62	44	50	29

$$\mu_2 = 76.3 \quad \sigma^2 = 160$$

$$\mu_1 = 52.8 \quad \sigma^2 = 47.5$$

$$\mu_0 = 47.0 \quad \sigma^2 = 9.6$$

$$\mu_4 = 21.7 \quad \sigma^2 = 48.2$$

For these 4 pmts,  $\sigma^2$  is different from the expected mean, this doesn't agree with the hypothesis that the count are Poisson distributed, we can quantify this with a statistical test: in this table the correlation matrix:

Pmt:	2	1	0	pmt in coincidence
$\chi^2_9$	19.6	8.30	1.90	39.5

The expected error for the result of this test is  $\sigma = \sqrt{2 * (n - 1)} \simeq 4$ . In this case we are observing 3 values that are more than  $3 \cdot \sigma$  far from the expected value. If we look at the correlation matrix :

pmt:	c	0	1	2
c	1	-0.18	-0.21	-0.06
0	-0.18	1	-0.10	-0.22
1	-0.21	-0.10	1	0.56
2	-0.06	-0.22	0.56	1

We observe negative correlation between the pmts, something not expected. After some investigations, we find out that the program which controls the NINO board had a bug: the program partially overwrote some detector B settings for detector A as well. Since detector B has only three pmt's, the problem affected the PMT's with the same numbering as detector A. After fixing this issue we repeated the same test, without finding any problem.

## 4.4 Calibrations.

One of the main goal for this experiment was to measure the well know trasverse asymmetry of  $^{12}C$ , already measured before, as a test for the new electronic system. Previous measurements of the Transverse asymmetry have been performed for a carbon target. For this beam-time, the two spektrometers were placed at an angle such that the  $Q^2$  values of the scattered electron is:

$$\begin{aligned} \text{Spektrometer } A : & \quad Q^2 = 0,041\,337 \text{ GeV} && \text{without Cut} \\ \text{Spektrometer } A : & \quad Q^2 = 0,039\,451\,3 \text{ GeV} && \text{with Cut} \\ \text{Spektrometer } B : & \quad Q^2 = 0,040\,477\,1 \text{ GeV} && \text{without Cut} \\ \text{Spektrometer } B : & \quad Q^2 = 0,040\,584\,3 \text{ GeV} && \text{with Cut} \end{aligned}$$

The  $Q^2$  values is the same of the last measurement performed at MAMI, and is measured with and without rejecting the inelastic electrons.

### 4.4.1 Alignment of the scattering plane.

### 4.4.2 Calibration of the VFCs monitors.

### 4.4.3 Beam monitors calibration.

For the calibration of the X Y monitors, we used two target made by three carbon wires at a certain distance from each other, aligned horizontally and vertically. The distance between the two center of the external wires is  $d_{horizontal} = 2,38$  mm for the target aligned horizontally and  $d_{vertical} = 2,33$  mm for the other one. With the two special targets aligned, we turn on the beam, asking MAMI operators to slowly change the beam position. The beam position can be changed by varying the Magnetic field produced by the *Wobbler 16* magnets (4.6):

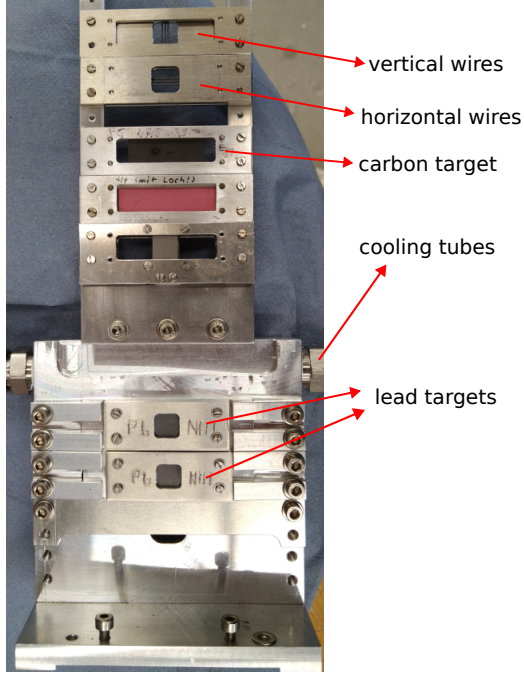


Figure 4.5: Target frame installed during the experiment, on the top we have the two targets made by three carbon wires that are used to calibrate the positions monitors. Then the carbon target and the two lead targets.

We took to acquisitions for horizontal and vertical wires target, changing the  $x$  and  $y$  position of the beam respectively. Looking at the PMT counts, we observe that the counts increase to a maximum, that is reached when the beam spot is centered on the carbon wire, and then decrease until the next carbon wire is hit by the beam.

We plot the pmt data *versus* the  $X_{25}, X_{21}, Y_{25}, Y_{21}$ , given in V. Given that we know the real distance between the two external wires, we can obtain the correct scaling factors to calculate the X and Y position from the voltage values. To identify the three peaks in of the carbon target, we fit the data using a gaussian model (see 4.7). The mean  $\mu$  represents the center of the wire, given in V.

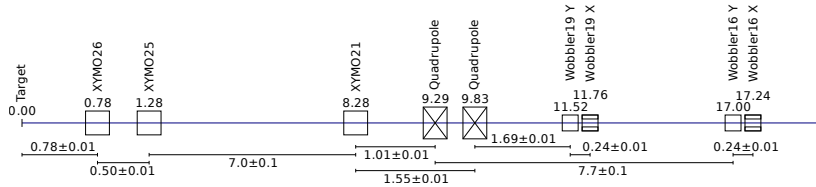


Figure 4.6: Beam line scheme.

Looking at the Beam line, we assume that the beam travels in a straight line. Let's consider the *Wobbler 16* magnet the "0" of a coordinate system, with the  $z$  axis pointing to the target (left direction in the beam scheme). The Beam parameters are measured by the Monitors  $X/Y_{21}, X/Y_{25}$ , which are located at some distance respect to the target. Suppose we are working only with the  $Y_{25}$  monitor (the procedure is the same for the others). The Beam  $y$  position is described by:

$$y_{beam} = m \cdot (z - z_{wobbler16})$$

In the scheme 4.6 we easily compute the distance between the  $Y_{25}$  monitor and the *wobbler 16* magnet, so we have the slope  $m$ . The Position on the target is given by  $Y_{target} = m \cdot Z_{target}$ . With these simple equations then:

$$c_{Y25} = \frac{d_{vertical}[\text{mm}]}{Y_{target}} \quad (4.5)$$

$c_{Y25}$  indicates the scaling factor of the monitor. With these values the Analysis program compute the correct beam position, and from that the incident angles in the  $x, y$  directions, which are needed later for the analysis.

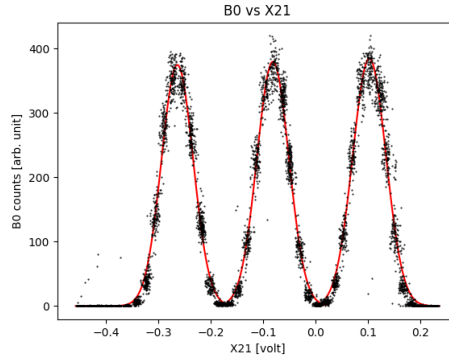


Figure 4.7

All this procedure can be easily checked if we plot now the  $X$  and  $Y$  position for the same two runs of data acquired with the wires. After placing the scaling factors obtained in the standard configuration file, we run the analysis another time and the physical values were computed 4.8

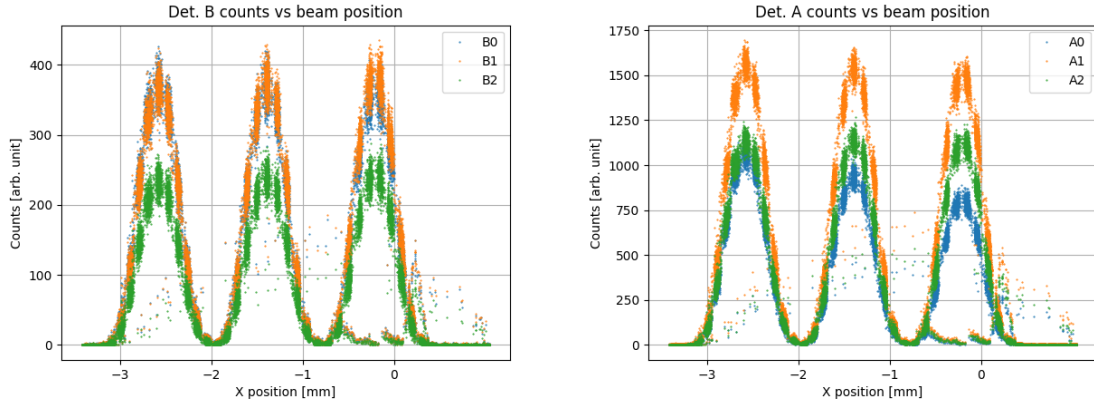


Figure 4.8: plot of the PMT Count against the physical values computed by the analysis program. Now the position of the three peaks correspond to the expected values measured for the target.

#### 4.4.4 Current (PIMO) and energy monitors (ENMO) calibration.

The last two calibration needed for the analysis are about the energy and the current intensity of the beam, which are indicated with PIMO (current monitor) and ENMO (energy monitor). The values that we measure are given by VFCs counts. We remind the reader how the VFCs monitors operate: the input signal from the beam is transformed in a pulse wave whose frequency is proportional to the input voltage. The signal is so proportional to various quantities that we want to measure, however we need to determine the correct scaling factor and possible offsets to convert these quantities in physical units ready for the analysis. For this beam time the current is measured in  $\mu\text{A}$  and the beam energy is given in eV.

For the current monitors I13 and I21, the raw counts are converted in digitalized voltage values with the formula shown in (3.8). The relation between these values given in V and the real values in  $\mu\text{A}$  and eV is linear:

$$I(\mu\text{A}) = mI(\text{V}) + q$$

To determine the two coefficients, the beam current was raised from  $10 \mu\text{A}$  to  $22 \mu\text{A}$  in several steps. For each step we confront the nominal values of the current, communicated by the MAMI operators which control the beam, with the values in V measured. The following plot shows the procedure described:

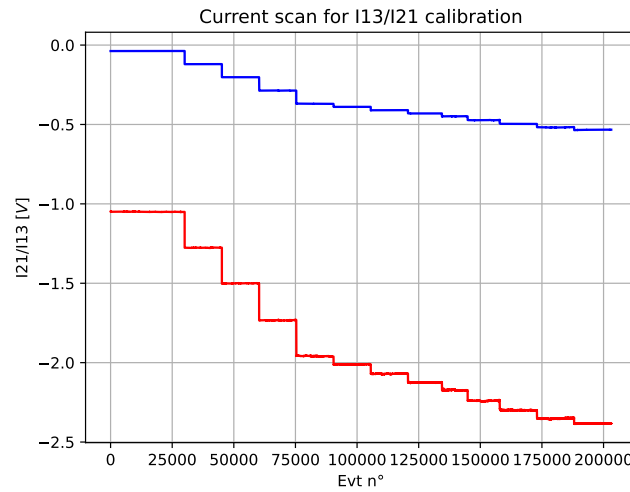


Figure 4.9: Current scan for the calibration, each step corresponds to a run with a different beam current.

The calibrations consist in retrieving  $m$  and  $q$  with a linear fit. Then the parameters are added in the standard configuration file, together with the other calibration parameters, and can be loaded by the analysis program to process the data.

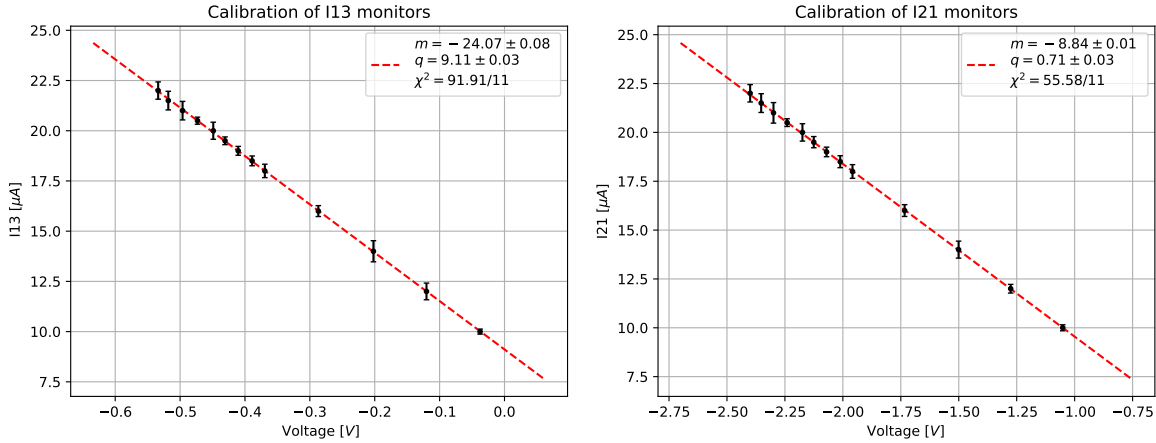


Figure 4.10: Calibration plots for PIMO I21 and PIMO I13, the errors are multiplied by 25.

The values obtained from the fit of nominal beam current vs. voltage values are shown in the figure 4.10. The  $\chi^2$  values are higher than the expected. This is not unexpected, the errors in both the plots are computed with the sampling standard deviation formula applied to the sequence of voltage values  $I21/I13$  ( $\sigma_{vfc}$ , the standard deviation computed for each step in 4.9), and it is related to precision of the analog to digital converter VFCs.

The errors are then propagated to the  $y$  axis showed in the plot. Yet, we are underestimating the error associated with nominal current  $I$ , in fact the accuracy associated with the beam current, set by the accelerator operators, was not disclosed, and we suspect that is not negligible compared to  $\sigma_{vfc}$ .

The ENMO calibration is performed in a different way from the other monitors. The polarity signal is sent to MAMI, and they produce a signal for the ENMO that somehow (need to investigate exactly how they do that) shows a difference between the first two sub-events and the last two. This difference is equal (nominal) to 22,6 keV. The idea now is to produce an histogram for the quantity  $\delta E$  (with  $E_{18}$  being the energy monitor):

$$\delta E = \frac{E_{18}[2] + E_{18}[3]}{2} - \frac{E_{18}[0] + E_{18}[1]}{2}$$

The data should be distributed with a peak around 22,6 keV. To obtain the correct scaling factor for the values stored in the data tree we plot the voltage values measured by the ENMO monitor. 3 runs of data were taken with different Beam current, to study the dependence of the measured quantity from the beam current. From the mean of the distribution it is possible to estimate the scaling factor for the ENMO monitors, obtaining the physical quantity in the following way:

$$C_{E18} = \frac{22.6 \text{ keV}}{\delta E}$$

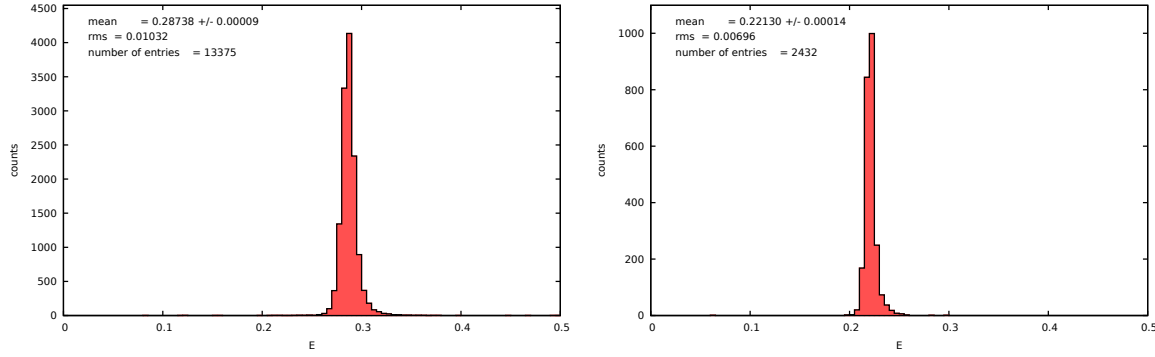


Figure 4.11:  $\delta E$  for 20 20  $\mu\text{A}$

Taking the average over  $E_{18}$  voltage values, and using the formula above, we obtain the coefficient  $C_{E18}$ . To take care of the current dependence of the monitors, the scaling factor to be placed in the standard.config file is:  $C_{E18}\bar{I}_{\mu\text{A}}$ . The calibration was performed taking three short acquisitions with different beam current : 20  $\mu\text{A}$ , 15  $\mu\text{A}$  and a run without beam.

Figure 4.12: Calibration of ENMO monitor

From this we obtain the value  $c_{E18} = -1595.2$  necessary to convert from Voltage units to keV the physical quantity for the analysis. As a final check the final histogram for the physical quantity is shown:

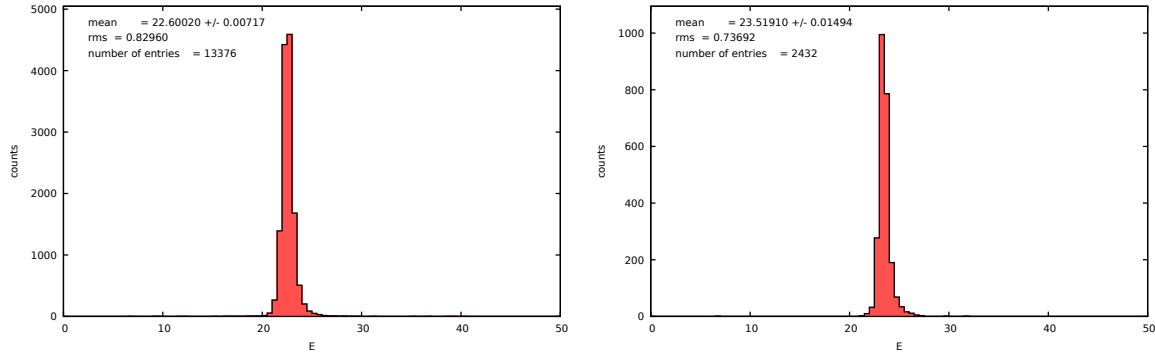
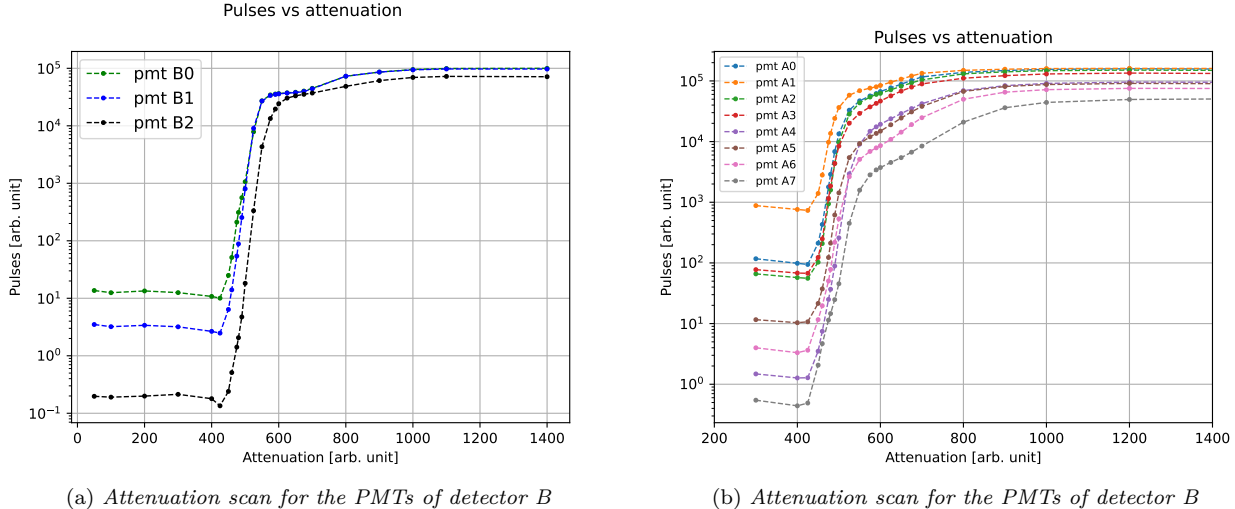


Figure 4.13: Plot for the physical quantities computed in the data tree, for two different current of the beam (on the left 20  $\mu\text{A}$ , 15  $\mu\text{A}$  on the right)

#### 4.4.5 Calibration of the PMTs

During the beam time, several scans in attenuation were performed, before switching MAMI to produce the polarized beam, to choose the best working point for the PMTS of the detectors. The same procedure used in the laboratory was followed, so with a beam intensity of  $10\text{ }\mu\text{A}$  we acquire data run one minute long, increasing each time the attenuation.



From the fit we obtain three values for the signal Peak, given in attenuaton units. We can check the idea behind this, visualizing the PMT count in a different way. Because we would like to visualize the number of electrons that generate a certain signal in the detector, we can think of differentiating the data showed in the plot 4.14a. The differentiation consist in the difference between the Counts at a certain point and the previous one, and dividing by the increment in attenuation:

$$Spectra = \frac{N(att_i) - N(att_{i-1})}{att_i - att_{i-1}}$$

In this way we compute a discrete derivative of the plot showed in 4.14a, which represent  $\frac{\partial N}{\partial att}$ . This is, in fact, the spectra of the signal, still given in attenuation units 4.14a.

This plot are used to identify a good point to select the attenuation values. If we look at the plots 4.4a, we can see that the physical threshold does not scale linearly with changing the attenuation value, and for high values of attenuation, the threshold falls quickly at zero. Looking at the signal spectra, we identify the first peak as the electron signal. The other peak, for higher attenuation values (on the right), correspond to very low threshold values, and it is identified as the background noise. We selected the values of the attenuation between the peaks of the two distributions, maximizing the signal acceptance and trying to reject the background as much as possible. Our discussion so far is sufficient to carry out the calibration of the PMTs and take data to measure the asymmetry. However, we would like to identify the physical threshold in mV instead of attenuation unit. We can use the conversion function that we discussed in 4.4a:

$$f(att) = \frac{a}{(x - b)^3 + d}$$

We point out that the parameters of this function have been obtained from data that have not been acquired during this thesis work, moreover the threshold value in the program that controls the NINO board is slightly different (we always used 600, the data are taken with 750), therefore the values in volts need probably to be rescaled by some factor, but for our discussion we are interested in a raw estimation of the signal peak: With this conversion, we show the same plots in 4.14a, with the values in the x-axis in V now.

We know see clearly two peaks, the signal and the background, that are reversed respect to 4.14a.

We discuss now a simple model that we used to describe how the PMT Counts vary when we raise the attenuation. From 4.14a, we assume that the two peaks are described by two gaussian distributions. Now if we think about the the probability for a signal to pass the selection, this quantity is equal to the probability of being in below the attenuation value. Using now the fact that the probability are given by the cumulative of the gaussian distribution (probability of being in the right tail) it is straightforward to deduce:

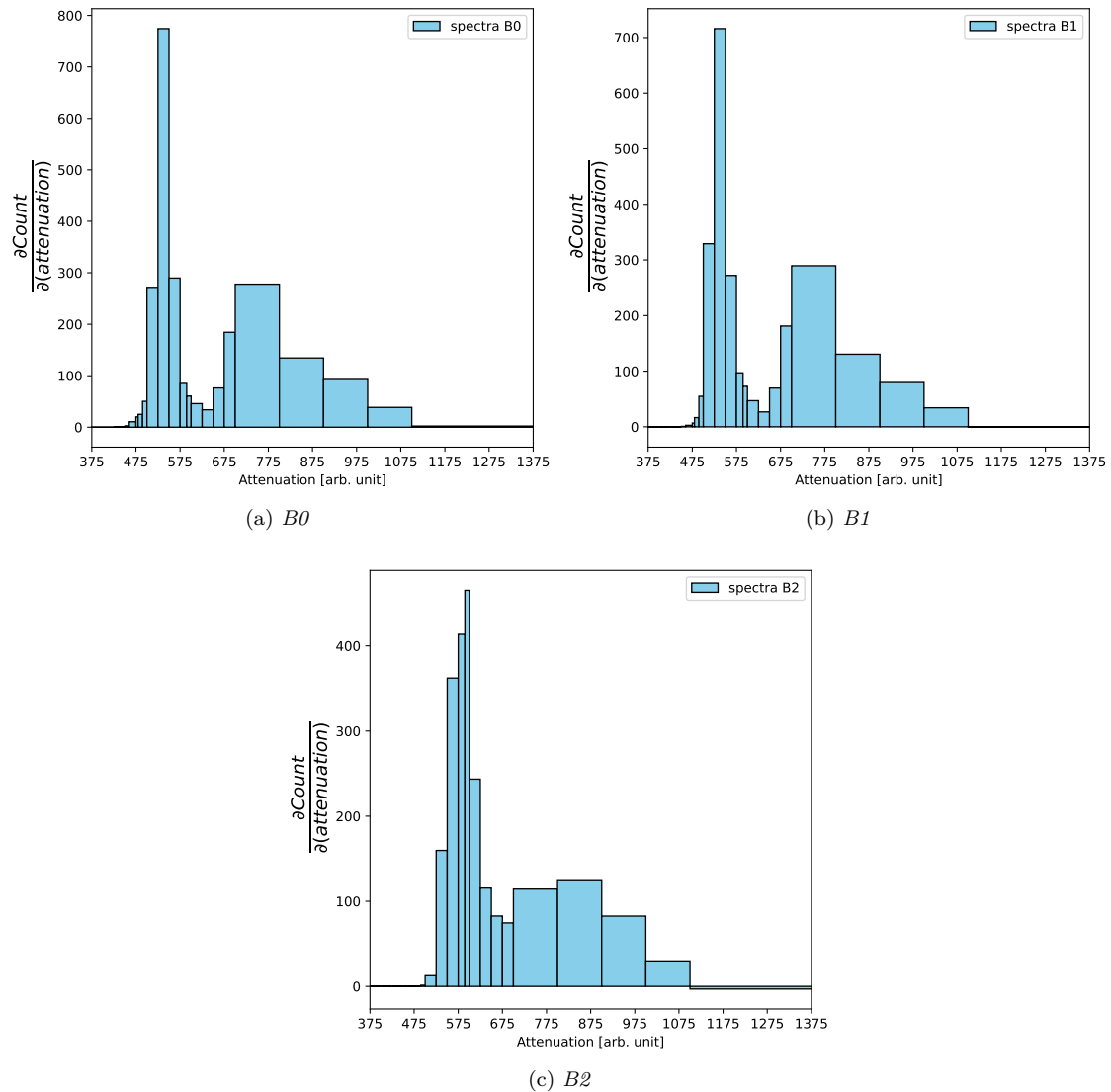
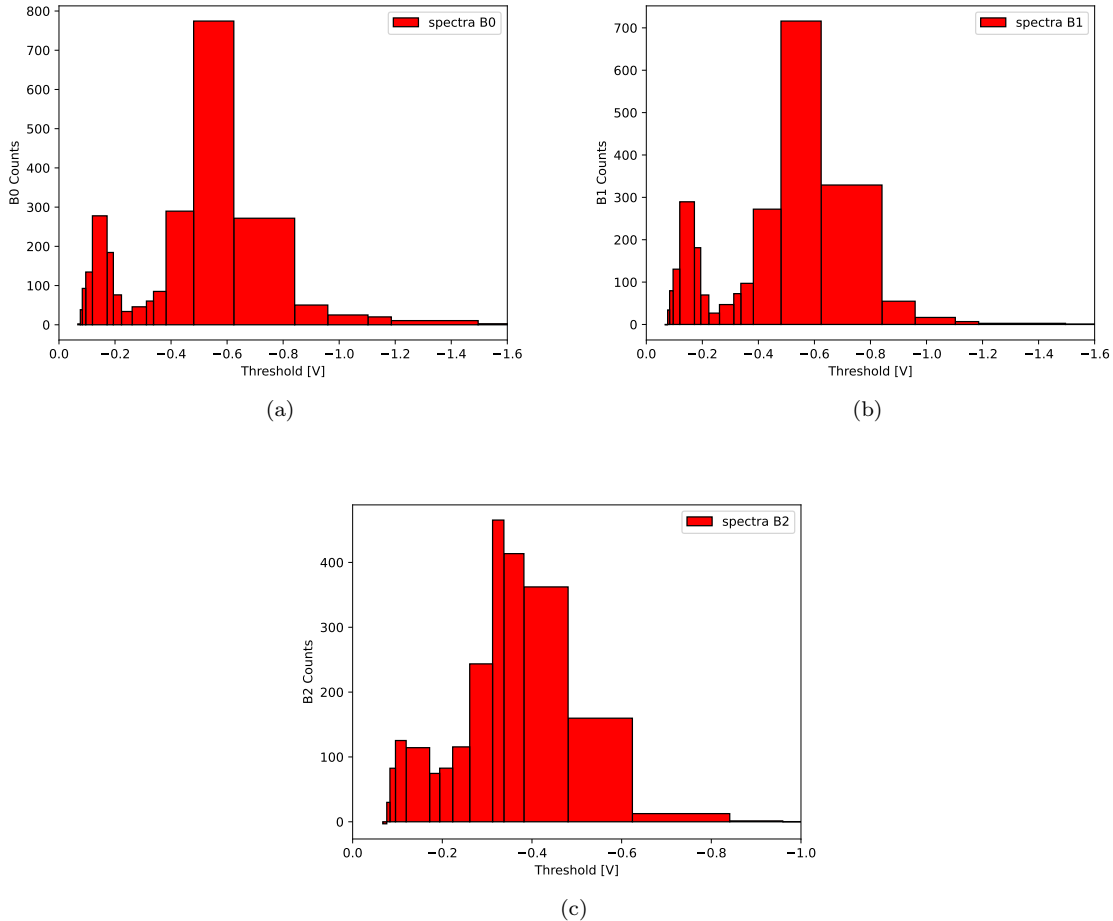


Figure 4.14: Recostructed spectra for Detector B



PMT	$\mu_1$	$\sigma_1$	$\mu_2$	$\sigma_2$	n1	n2
B0	538.0 +/- 1.3	19.4 +/- 1.1	798 +/- 8	103 +/- 4	34277 +/- 662	64244 +/- 1538
B1	536.4 +/- 0.9	18.2 +/- 0.7	783 +/- 5	89 +/- 2	34053 +/- 475	61636 +/- 1109
B2	582.8 +/- 1.2	25.9 +/- 1.0	824 +/- 8	88 +/- 6	32880 +/- 758	37930 +/- 1245

$$P(signal > thr) = \Phi(x) = \frac{1 + Erf(\frac{x - \mu}{\sqrt{2}\sigma})}{2}$$

Considering that we have the sum of two gaussian distribution, we end with:

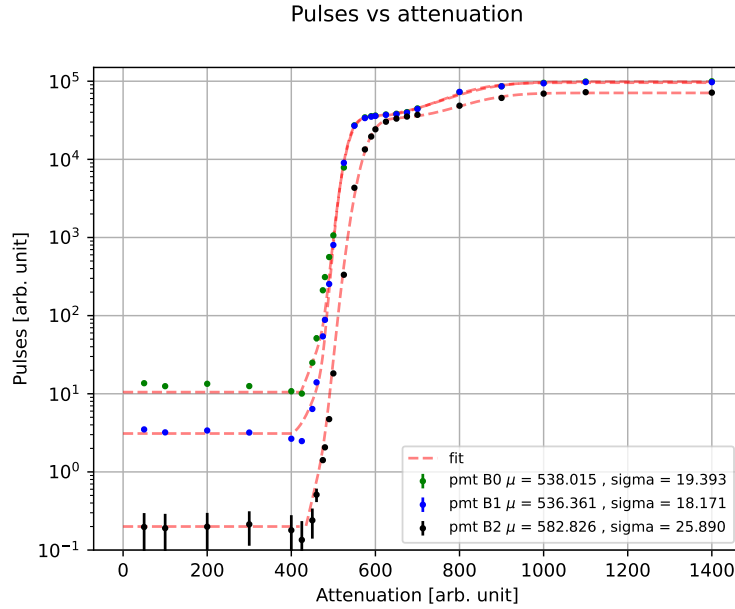
$$N(att) = \frac{n_1 + n_2}{2} + \left(\frac{n_1}{2}\right)Erf\left(\frac{x - \mu_1}{\sqrt{2}\sigma_1}\right) + \left(\frac{n_2}{2}\right)Erf\left(\frac{x - \mu_2}{\sqrt{2}\sigma_2}\right) \quad (4.6)$$

This model is used to fit the data. The result is shown in the following picture, the parameters obtained from the fit are reported below:

From these result we measure the mean  $\mu_1$  and  $\mu_2$  for the signal and the background given in attenuation units. The correct value of attenuation is set between the two observed peaks, in order to rejects the background and take only the signal coming from the scattered electrons. The same procedure was followed also for the detector A, the plots are not reported here, for brevity, but in the appendix.

#### 4.4.6 Autocalibration procedure

In this section we present the last calibration techniques needed in the data-process. The autocalibration is a special operation mode of the MAMI accelerator, during which the beam current is made to vary in a controlled way. Through these special runs it is possible to obtain again the current scaling factor that we discussed in 4.3.4. Because the current is varying, it is possible to study the linearity of the PMTs. From a linear fit of the



PMTs counts vs. current intensity the angular coefficient and the offset are measured. The offset is particual important because give rise of a possible systematic error that influence the final asymmetry result. It is quite simple to demostrate this, if a relation of the type  $N = mI + N_0$  holds. Consider the following quantity:

$$\bar{N} = \frac{N_{\uparrow} + N_{\downarrow}}{2}$$

we can express  $N_{\uparrow}$  and  $N_{\downarrow}$  in this way:

$$\begin{aligned} N_{\uparrow} &= \bar{N} + A_n \bar{N} \\ N_{\downarrow} &= \bar{N} - A_n \bar{N} \end{aligned}$$

Now we suppose that  $\bar{N}$  is linear dependent on the current in the way we defined above, so:

$$\begin{aligned} N_{\uparrow} &= \bar{N} + A_n(\bar{N}) + N_0 \\ N_{\downarrow} &= \bar{N} - A_n(\bar{N}) + N_0 \end{aligned}$$

We are supposing that the offset  $N_0$ , we assume that the present offset does not contribute to the asymmetry, i.e. it is not correlated to the signal of the scattered electrons, but is due to processes of another type, therefore in the previous formulas only the  $mI$  counts must be multiplied by the asymmetry  $A_n$ . Therefore if we substitute everything in the definition of the transverse asymmetry:

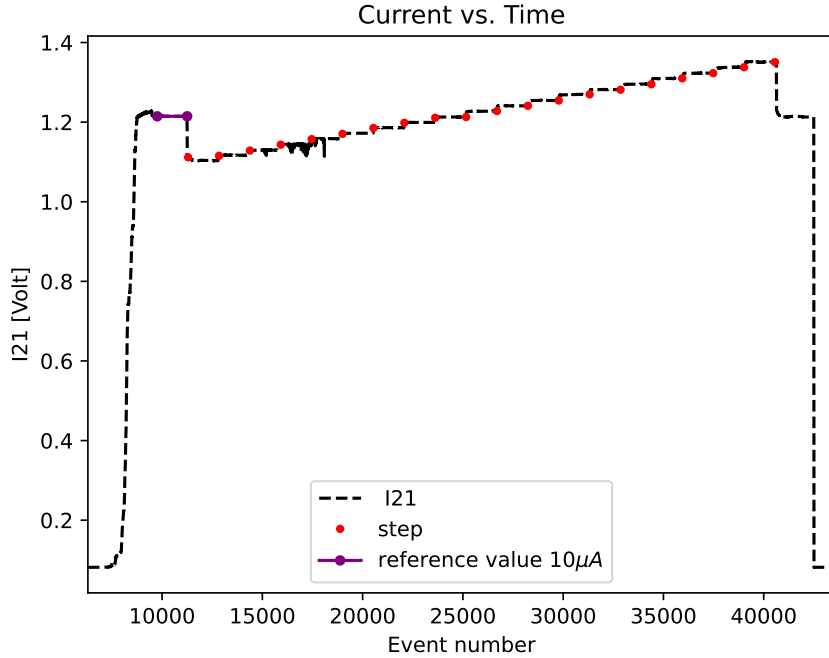
$$A' = \frac{N_{\uparrow} - N_{\downarrow}}{N_{\uparrow} + N_{\downarrow}} = \frac{A_n(2mI)}{(2mI) + 2N_0} = A_n \frac{1}{1 + \frac{N_0}{mI}} \quad (4.7)$$

In the last passage we learn that the presence of an offset can decrease the reconstructed asymmetry. So it's important to determine quantitatively  $N_0$  and  $m$  in order to be able to take care of this effect. The strategy used is quite simple: every three hours of production data, we asked MAMI to start the autocalibration program. With all the autocalibration runs, we estimate  $N_0$  for each PMT, separately. Then All this quantities are saved in a file so that the analysis program can retrieve the parameters and subtract them from the PMT counts. In

this way every three hours the PMT are corrected, this take care also of the possibility that the the linearity of the PMTs can change after hours of use of the PMTs (for example it can decrease the efficiency).

During the autocalibration, the beam current is raised from 9  $\mu$ A to 11,125  $\mu$ A in step of 0,125  $\mu$ A:

With a linear fit we can estimate the scale and the offset to convert from I21 voltage values to physical values of the current. The procedure is repeated for the 8 autocalibration acquisition we had during the beam time, so we can also take care of possible variations during the time.

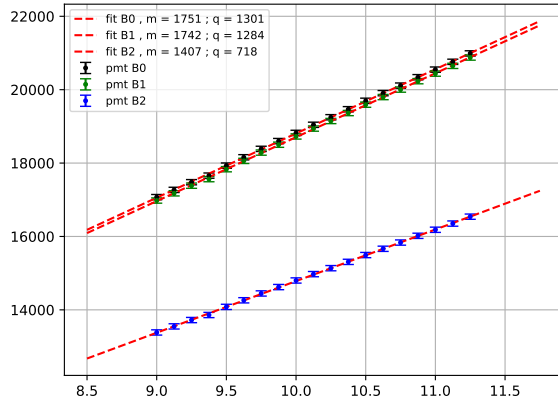


(a) Autocalibration: in this plot we have the voltage value of  $I_{21}$  monitor. The current is first stabilized around  $10\text{ }\mu\text{A}$ , then it is raised from  $9\text{ }\mu\text{A}$  (the step lower down) to  $11,125\text{ }\mu\text{A}$  in step of  $0,125\text{ }\mu\text{A}$ .

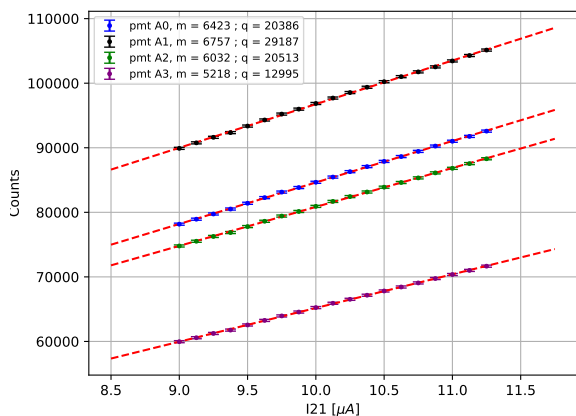
The figures are referred to the data acquired for the first autocalibration. It's interesting to calculate, from the result of the fit, the factor that appears in 4.7:

PMT	$m [\mu\text{A}^{-1}]$	Offset	c
B0	1750	1301	0.93
B1	1742	1283	0.93
B2	1406	717	0.95
A0	6423	20385	0.75
A1	6756	29187	0.70
A2	6032	20513	0.75
A3	5218	12995	0.80
A4	3945	6666	0.86
A5	3967	6547	0.86
A6	3258	4655	0.87
A7	2325	2233	0.91

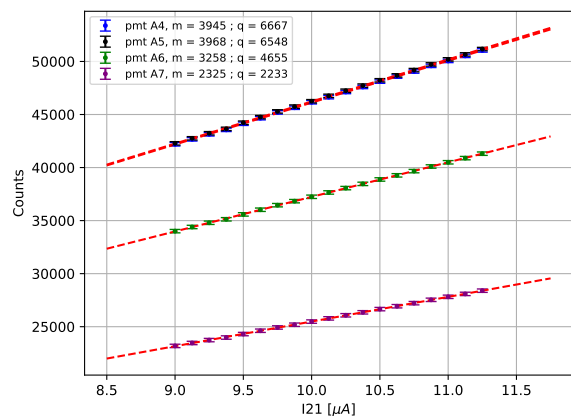
Ignoring the presence of the offset lead two consequences: the reconstructed asymmetry is lower, on average  $\simeq 10\%$  less than expected, and the Counts are overestimated. Because the error depend on the PMT counts, as seen in 2.7, this two effect combined add up and worsen the precision and accuracy of the measurement. The result reported in the table can be confronted with the final result that are reported in 6.



(a) Current scan for detector B, the error are multiplied by a factor of 20.



(a) Current scan for detector A, the error are multiplied by a factor of 20.



(b) Current scan for detector A, the error are multiplied by a factor of 20.

Figure 4.15: PMT Rates vs current (from I21 monitor), the model used for the fit:  $y = mx + q$ .

# Chapter 5

## Asymmetry on Carbon and Rates on Lead target.

**introduction** After having described all the calibrations needed, we are ready to analyze the data and measure the transverse asymmetry from the data collected in second part of the beam time. In this chapter we explain the procedure for the pre-selection of the data (for example the removal of the events with large variation of the beam parameters) and the procedure used to analyze the reconstructed asymmetry in order to obtain in the end a point estimation for  $A_n$ . A section is dedicated to the measurement performed with lead target: the experimental rates measure using the detectors setup described here () are reported; through the knowledge of the expected counts per sub-event, we calculate the amount of statistics needed to measure the transverse asymmetry on  $Pb$  with an accuracy of 1ppm. In the end we discuss the problem of the false asymmetries that can affect the final result, and also a raw estimation of the systematic error is performed, in the end.

### 5.1 Rates on lead

After all the calibrations are finally performed, the experimental setup is ready to take real "production" data to achieve the objectives of the experiment. The first goal of the experiment is to measure the rates on  $Pb$  target. The lead target installed is made by a thin layer with a thickness of 0,5 mm, and it's not isotopically pure. The expected rates are given by the Mott cross section, that we report here .

We took 14 acquisitions lasting  $\simeq 2,5$  minutes, which corresponds to 6950 events. For each of these acquisitions we set the beam current at different values, ranging from  $10 \mu\text{A}$  to  $22 \mu\text{A}$  of intensity. The Rates are then reported as a function of the current, a linear model is used to fit the data.

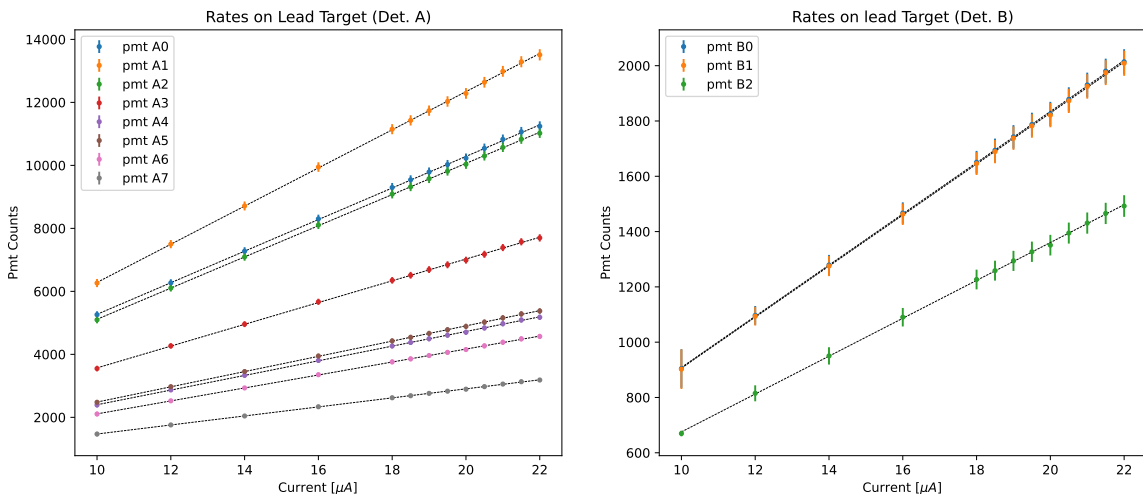


Figure 5.1: Rates on lead Target in function of the beam current. The Rates for each PMT of detector A (on the left), and detector B (on the right) are reported.

The angular coefficient  $m$  and the offset  $q$  are reported in the table below.

In this other plot we show the residuals: .

PMT	m [ $\mu\text{A}$ ]	q	$\chi^2$ (dof = 9)
A0	501.42 +/- 2.17	256.55 +/- 39.57	13.7521
A1	605.77 +/- 2.31	226.11 +/- 42.04	13.3783
A2	495.01 +/- 1.47	163.04 +/- 26.83	6.95713
A3	345.68 +/- 1.6	113.4 +/- 29.16	12.1727
A4	232.58 +/- 0.9	74.38 +/- 16.44	5.36892
A5	241.95 +/- 0.74	65.79 +/- 13.51	3.48398
A6	205.79 +/- 0.65	52.38 +/- 11.87	3.0892
A7	143.42 +/- 0.47	36.49 +/- 8.55	2.26341
B0	92.55 +/- 0.34	-16.88 +/- 6.16	2.05286
B1	92.29 +/- 0.33	-16.9 +/- 5.97	1.92163
B2	68.48 +/- 0.32	-9.34 +/- 5.91	2.81988

The PMT Counts with this target, increase from 100 counts for detector B to 500 counts every  $1 \mu\text{A}$ . The experimental error  $\sigma$  related to the asymmetry was studied in , we recover the formula:

$$\sigma = \sqrt{\frac{1}{2N \cdot n}} \quad (5.1)$$

we remind to the reader that  $N$  are the Counts per sub-event, while  $n$  is the number of event analyzed. Now estimate the amount of statistic needed to measure the asymmetry with some degree of accuracy. Let's suppose that we want to obtain, for each PMT, an error not greater than  $4\text{ppm}$ . With this accuracy, the asymmetry obtained for detectro A will have an error given by  $\frac{4\text{ppm}}{\sqrt{n_{PMT}}} \simeq 1.5\text{ppm}$ . We computed the time needed to achieve this accuracy for both the two detectors, given in total hours of beam-time. To simplify the calculation, we assumed that every PMT rates of detector A and B are equal to the averaged counts obtained from the plot above.

current I	T [h] Det A	T [h] Det B
10	344	1487
12.5	277	1185
15	232	985
17.5	199	843
20	175	737

As we will see in the next part of this chapter, focused on the asymmetry on carbon target, the amount of time needed to obtain an accuracy of  $\simeq 1.5\text{ppm}$  is roughly  $15h$  with  $10 \mu\text{A}$ . The same measurement with lead will need 23 times the statistic accumulated for Carbon. This involves more experimenta difficulties:

- deterioration of lead target.
- need to develop a target cooling system.
- monitor the radioactivity levels in the experimental hall.

## 5.2 Model for fitting the data

One of the problems of the measurement is to take into consideration the various contributions that can change the value of the asymmetry measured by the experimental apparatus. The raw values of the asymmetry can be affected by the variation of the beam parameters during the time. Let's summarize quickly all these effects:

- the PMTs counts can depend on the  $(x, y)$  impact position of the beam on the target
- the variations of the incident angles  $\theta_x$ and  $\theta_y$  on the target.
- the uncertain associated with the energy of the Beam, a change in the energy associated with the polarization of the beam leads to different rates for the cross section
- the uncertain associated with the current of the Beam, in particular a change due to the efficiency of the source in producing electrons polarized in the two opposite directions

All this quantity, which we will indicate in general with  $\delta q$  can influence the asymmetry measured by the PMTs, considering also that the expected asymmetry is in the order of ten part per million, and small asymmetry introduced by fluctuations on the beam parameters are not negligible. Correcting directly the false asymmetries that rise from those uncertainties is a tough task, and it's more easy to adopt a different strategy respect to proceed to the analytical/numerical calculation of each of them. Knowing that the beam parameters produced by Mami are quite stable over the time, we can assume that the measured asymmetry are well described by a linear model as the following:

$$A_{tot} = A_{physical} \cdot P + \delta_I + A_x \delta x + A_y \delta y + A_{\theta_x} \delta \theta_x + A_{\theta_y} \delta \theta_y + A_E \delta E \quad (5.2)$$

$A_{physical}$  is the aim of the experiment,  $A_x$  and  $A_y$  are the asymmetries induced by the variation of the position of the beam,  $A_{\theta_x}$  and  $A_{\theta_y}$  are the asymmetry associated to angles,  $A_E$  is the asymmetry associated to the beam energy. The relevant assumption is that, for small variation of the beam, the false asymmetries are linearly dependent on the Beam uncertainties (that are  $\delta x, \delta y, \delta \theta_x, \delta \theta_y, delta_E$ ), so a first order approximation seems valid.

We must clarify now what we mean with  $\delta x, \delta y, \delta \theta_x, \delta \theta_y, delta_E$ . Resuming the event structure, that we discussed in 3.1, we have a sequence of 4 different sub-events, with a polarization pattern that is randomly selected between  $\uparrow, \downarrow, \downarrow, \uparrow$  and  $\downarrow, \uparrow, \uparrow, \downarrow$ . During the 20 ms of time length of each sub-event, the vfc's make a single measurement of the beam, and the data are saved in the data tree. The task of the analysis program is to use this raw data to calculate the relevant parameters for the analysis. Because we are working with asymmetries, the absolute values of the parameters listed above is not relevant, instead what is relevant are the differences correlated with polarization state of the beam. Assuming this,  $\delta x, \delta y, \delta \theta_x, \delta \theta_y, delta_E$  are replaced with :

$$\begin{aligned} \delta x &= \left( \frac{X_{\uparrow}(1) + X_{\uparrow}(2)}{2} \right) - \left( \frac{X_{\downarrow}(1) + X_{\downarrow}(2)}{2} \right) \\ \delta y &= \left( \frac{Y_{\uparrow}(1) + Y_{\uparrow}(2)}{2} \right) - \left( \frac{Y_{\downarrow}(1) + Y_{\downarrow}(2)}{2} \right) \\ \delta E &= \left( \frac{E_{\uparrow}(1) + E_{\uparrow}(2)}{2} \right) - \left( \frac{E_{\downarrow}(1) + E_{\downarrow}(2)}{2} \right) \\ \delta \theta_x &= \left( \frac{\theta_{x,\uparrow}(1) + \theta_{x,\uparrow}(2)}{2} \right) - \left( \frac{\theta_{x,\downarrow}(1) + \theta_{x,\downarrow}(2)}{2} \right) \\ \delta \theta_y &= \left( \frac{\theta_{y,\uparrow}(1) + \theta_{y,\uparrow}(2)}{2} \right) - \left( \frac{\theta_{y,\downarrow}(1) + \theta_{y,\downarrow}(2)}{2} \right) \end{aligned} \quad (5.3)$$

Each  $\delta q$  represents the variation of one of the parameters of the beam within an event, so. One may wonder why the model doesn't contain a parameter  $A_I$  to describe the false asymmetry due to the current. We can show theoretically that the values of  $A_I$  is equal to 1. Starting from the definition of rate  $\Gamma$ :

$$\Gamma = \frac{dN}{dt} = I_0 \sigma \frac{n_t}{S} \quad (5.4)$$

where  $I_0$  is the beam current,  $n_t$  is the density of the target, and  $S$  is the surface of the beam. If we substitute everything in the definition of  $A$ :

$$A_I = \frac{\frac{dN_{\uparrow}}{dt} - \frac{dN_{\downarrow}}{dt}}{\frac{dN_{\uparrow}}{dt} + \frac{dN_{\downarrow}}{dt}} = \frac{\sigma_{\uparrow} I_{0\uparrow} - \sigma_{\downarrow} I_{0\downarrow}}{\sigma_{\uparrow} I_{0\uparrow} + \sigma_{\downarrow} I_{0\downarrow}} \quad (5.5)$$

It should be clear now that the current asymmetry  $A_I$  is equal to 1, and to take care of the contributions of the current we only need to compute  $\delta_I$ :

$$A_{tot} = A_n + \frac{I_{0\uparrow} - I_{0\downarrow}}{I_{0\uparrow} + I_{0\downarrow}} = A_n + \delta_I$$

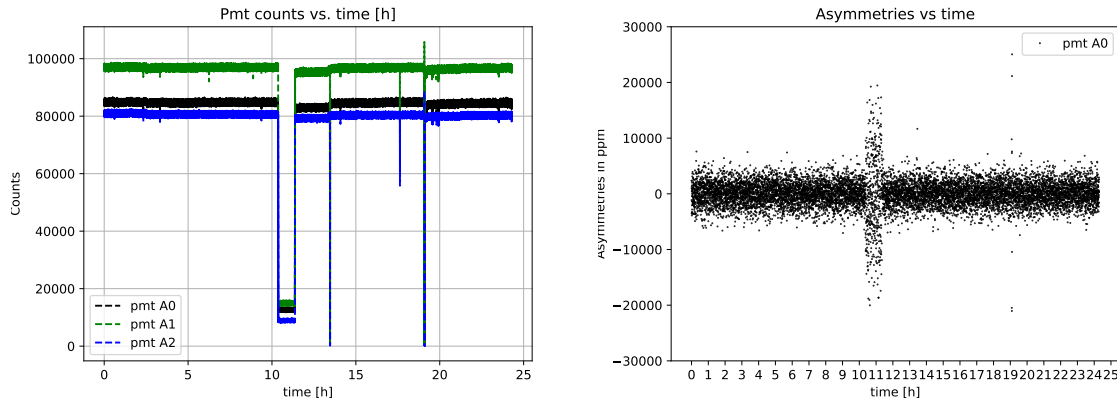
This is a direct consequence of the fact that the luminosity is proportional to the beam current, so we don't need to add a new parameter to the model.

### 5.3 Data pre-selection and Fit

After all the calibration are performed, the analysis program is ready to produce the data-files suitable to analyze the asymmetry data for Carbon.

The Data file that are produced from the binary files are simply files in txt format, where the data are stored

in columns. Before proceeding with the linear fit, however, it is necessary to visualize the data to check that there are no anomalous behaviors. In fact the data can contain moments of loss of the beam current and sudden interruptions, loss of polarization of the beam and even setting errors by MAMI operators can affect the experiment. Carbon data were taken from November 2nd to 4th, and consist of 28 runs, each 1 hour long. The first step is to observe the PMT counts and the current trend, in order to be able to identify sudden interruptions of the beam, outliers and to check the behaviour. Here we show the trend over time for the series runs:



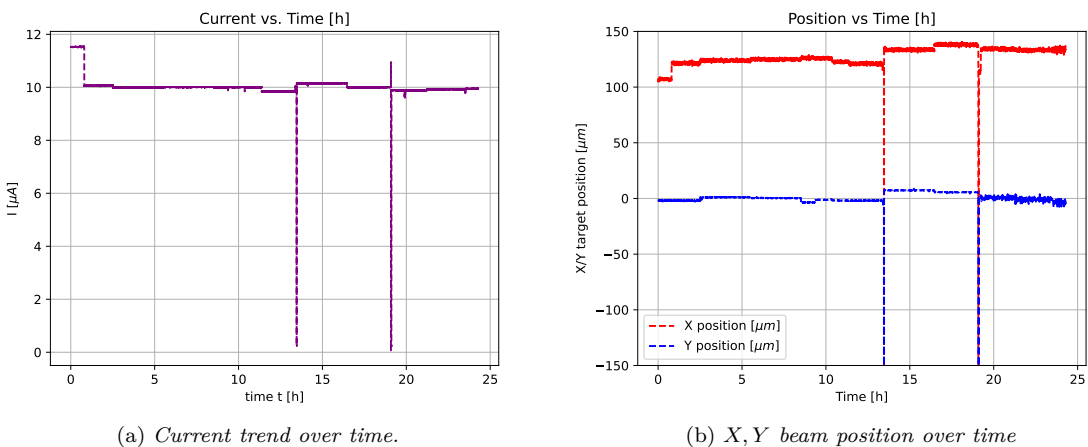
(a) *Counts vs. time*, the plot represent the Count trend versus time, made for all the runs acquired during the beam time. The conversion from event number to time is made knowing that each event correspond to 80 ms. A total of 22 hours of beam was collected.

(b) *Asymmetry trend for PMT A0*

This plot show that after 10 h of data acquisition the PMT counts (5.2a) dropped rapidly. If we show the current trend over the time (5.2a) we do not see a corresponding decrease in beam intensity. Also the  $x, y$  position (5.2b) and the energy monitor of the beam do not show a strange behavior, so we reject the possibility that the beam was not properly aligned to the target.

We have the strong suspect that this issue come from a failure to be attributed to the NINO board. In fact for all the PMTs, during that time interval, the counts are equal to the offsets measured with the auto-calibration run. Our suspect is that the threshold and attenuation settings that are loaded during the initialization of the DAQ program were not set correctly. For the analysis, those data are rejected completely.

Apart from this, we observe in (4) sudden variations of the asymmetry around 13.5h and 19h, that correspond to decreases in the plot on the left. We reject these data because we observe the same variation also for the current monitor, which means that the beam intensity fall quickly to 0 for a short period of time.

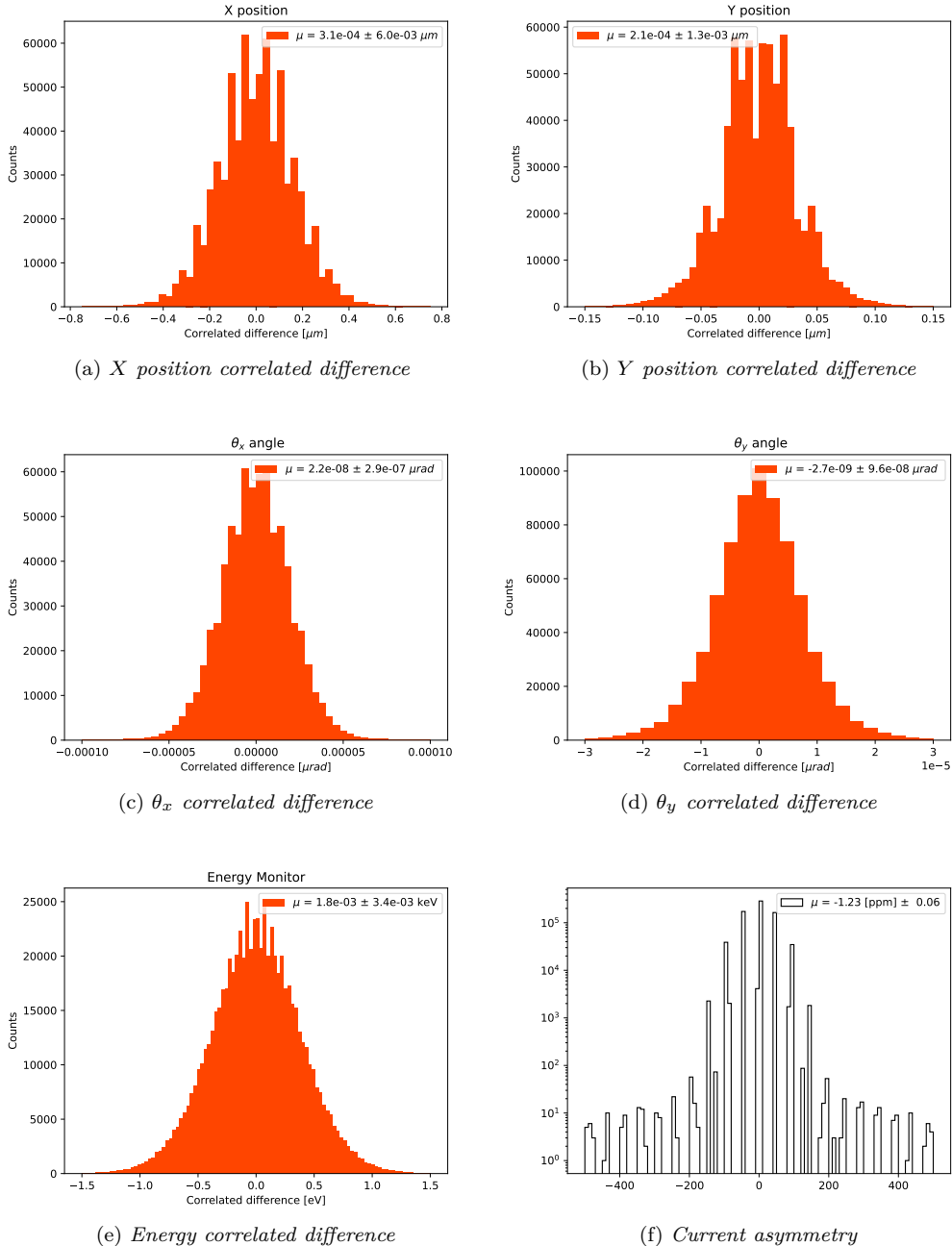


(a) *Current trend over time.*

(b) *X, Y beam position over time*

Now we focus our attention on the correlated-difference values. We remind the reader that these quantities, that are used as independent variables for the fit, as explained before, are defined as

$$\delta x = \frac{(x_{up,1} + x_{up,2})}{2} - \frac{(x_{down,1} + x_{down,2})}{2}$$



and are calculated within each single event, to identify the differences with respect to the various quantities such as position, energy... which correspond to different states of polarization. Several histograms are produced (5.2a). These plots are useful to quantify the stabilization of the beam: we expect that all the correlated differences are distributed around zero, which implies that there is no systematic difference when the beam has one polarization state respect to the other. The mean  $\mu$  and the standard deviation  $\sigma$  of the data are reported in the table (5.1)

Looking at the values of the mean and the corresponding error  $\sigma$  reported in the plots legend, we observe that mean of  $X, Y, \theta_x, \theta_y, E$  are compatible with 0, except for the current correlated-difference, whose values reported already in *ppm* is significantly different from zero. These results are encouraging: we are not able to identify a systematic difference between polarization +1 and -1. A systematic difference would have produced a value  $\mu$  shifted from zero, and a corresponding effect on  $A_n$ . With our assumption that the false asymmetries are well described by a linear model, observing that  $\mu$  is small and compatible with zero for all the parameters, together with the evidence that  $\delta q$  are distributed symmetrical around zero, it could be stated that by averaging the asymmetries:

Table 5.1: Beam parameters:

	Beam Parameters: $X[\mu\text{m}]$	$Y[\mu\text{m}]$	$Xp[\mu\text{rad}]$	$Yp[\mu\text{rad}]$	$E[\text{eV}]$	$I[\text{ppm}]$
$\mu$	$1.31 \cdot 10^{-3}$	$2.4 \cdot 10^{-4}$	$3.2 \cdot 10^{-8}$	$3.6 \cdot 10^{-9}$	0.0013	-1.23
$sigma$	$3.7 \cdot 10^{-1}$	$2.9 \cdot 10^{-2}$	$1.9 \cdot 10^{-5}$	$6.5 \cdot 10^{-6}$	0.38	50.4

$$\begin{aligned} \bar{A} &= A_n \cdot P + \overline{\delta_I} + \overline{\delta_x} A_x + \overline{\delta_y} A_y + \overline{\delta_{\theta_x}} A_{\theta_x} + \overline{\delta_{\theta_y}} A_{\theta_y} + \overline{\delta_E} A_E = \\ &= A_n \cdot P + \overline{\delta_I} + A_x \cdot 0 + A_y \cdot 0 + A_{\theta_x} \cdot 0 + A_{\theta_y} \cdot 0 + A_E \cdot 0 = A_n \cdot P + \overline{\delta_I} \end{aligned}$$

The contributions related to the false asymmetry should in principle cancel out. We will discuss later, when we will introduce the fit results, whether our assumption reflects the reality. For now let's assume that the only false asymmetry that has an effect is the current false asymmetry, so the final result should be corrected subtracting the values  $-1.23 \text{ ppm}$ .

After discussing the removal of the outliers, now will discuss in details the issue regarding the polarization of the Beam. To observe a transverse asymmetry, it is essential to have a correctly polarized beam. Unfortunately, we found out that part of the data where acquired with a Beam made by non-polarized electrons. The reason is that during the second night of the beam-time, MAMI operators that controls the quality of the beam switched from polarized beam to non-polarized, unintentionally. These wrong data were acquired during the night of 2nd December and we discovered this problem only the next day. We had no evidence of how many hours of beam were lost. Because this happened during the night, nobody could save the polarization measurement of the beam and identify the runs affected by this problem. This issue introduces a big systematic error that is potentially decreases the reconstructed  $A_n$ . It is important to identify the runs that share this problem, otherwise the measurements are affected by a bias that is not possible to disentangle from any other systematic effects related to the electronics system of the experiment, therefore also the electronic testing is not possible. All the stabilization monitors were active, so the data show apparently the same behaviour of the data with the correct polarization. We can't proceed with an arbitrary cut of the data, because there is the risk to cut off also good data or perform an incomplete removal. The next phase of the analysis is focused on describing a clear method used to identify the data and remove them from the analysis.

The procedure to identify the runs with 0% polarization rely to the estimation of the correlation coefficient of the PMTs counts. For every event we have two type of polarization sequence. The polarization  $\vec{P}$  of each sub-event is identified with  $+1$  and  $-1$ , that correspond to up and down  $\vec{P}$ . This values are part of the data tree, and form a sequence  $p_i$  of the type:  $+1 - 1 - 1 + 1$ , where  $i$  is the index to the  $i$ -th sub-events analyzed. If the  $\vec{P}$  is different from zero, we expect, due to the transverse asymmetry, a difference in the number of scattered electrons between sub-events with different  $p_i$ .

sub-event	1	2	3	4	5	6	7	8
Polarity	+1	-1	-1	+1	+1	-1	-1	+1
PMT B0	101	99	98	102	100	99	97	103
PMT B..	...	...	...	...	...	...	...	...

Table 5.2: Example of the Polarity sequence and PMT counts that are saved in the analysis program. The values of the PMT counts given are for example.

This lead to a positive/negative correlation between the sequence  $p_i$  and the PMT data. In case of  $\vec{P} = \vec{0}$ , the expected values for the correlation should be zero.

We applied this strategy with the hope to identify and remove the block of data with  $A_n \simeq 0$ . The correlation  $c$  between the  $p_i$  and the PMT sequence  $N_i$  of counts is computed every  $t = 1h$ , that correspond to 45000 events. We plot the averaged correlation for detector A and B, and the correlation of the two detectors together (with the reverse sign for detector B).

The correlations coefficient  $c$  is clearly dependent on the  $\vec{P}$ . If we observe that  $c$  is compatible with zero, we have an evidence of the block of runs to be removed from the analysis. The values are reported in figure 5.2. The errors for each point are computed with the formula:

$$\sigma_c = \sqrt{\frac{1 - c^2}{N - 2}}$$

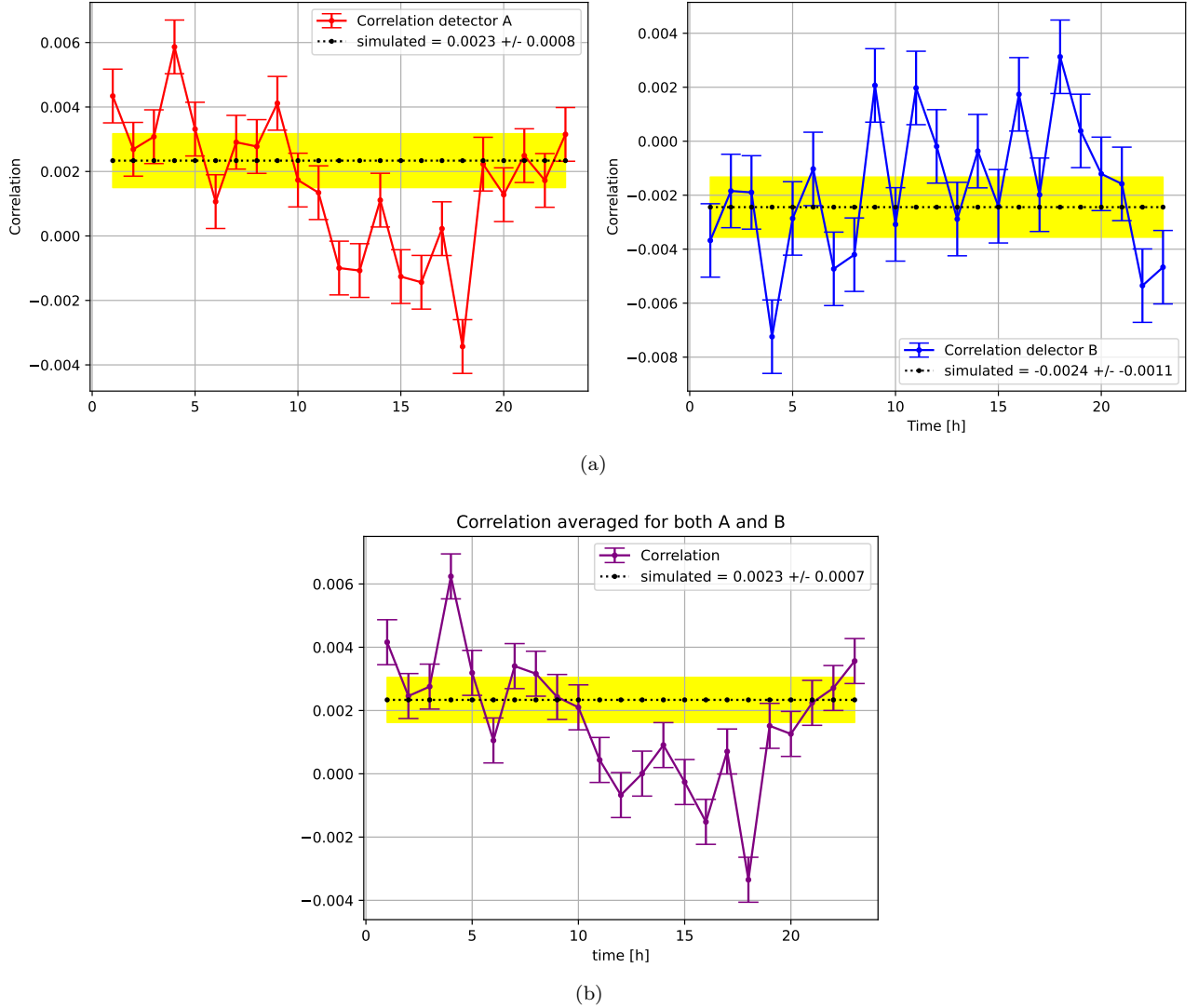


Figure 5.2: Plot of the correlation for detector A and on the left, and combining the two detectors results on the right. It's possible to identify a block of run starting at time  $t = 12h$  until  $t = 19h$  where the correlation is small and compatible with 0. The values can be confronted with the montecarlo, whose error band is in yellow.

The plots show also the expected values for the  $c$  computed with a simple simulation, using the values of  $A_n = 22.5\text{ppm}$  and  $P = 0.79$  as an input. The simulation results are obtained following these steps:

- A sequence of the type  $+1, -1, -1, +1$  is generated, long 45000 events.
- For each sub-event of the previous sequence, the PMT counts are generated: the counts are sampled from a gaussian distribution with  $\mu$  and  $\sigma^2$  equal to the values measured for both the detectors. To reproduce the correlation with the polarity sequence, the values are shifted accordingly by a factor  $\mu \cdot A_n \cdot P$
- The previous step is repeated 25 times, and for each iteration we compute and save the correlation between the polarity sequences and the counts.
- From the values saved, we compute the mean  $c$  (the dotted line in plot 5.2) and  $\sigma_c$ .

Looking at the plots, we observe for detector A a block of runs where  $c$  is compatible with 0, in contrast with the values expected from the simulation. Due to the higher error, the corresponding plot for detector B is not clear to interpret, however the plot on the right with the overall results for A and B confirms the evidence for A. This let us to identify the block of runs that show a behaviour compatible with  $\vec{P} = \vec{0}$ . It's important to double check that validity of this method seeing if the corresponding asymmetry is compatible with 0 5.3.

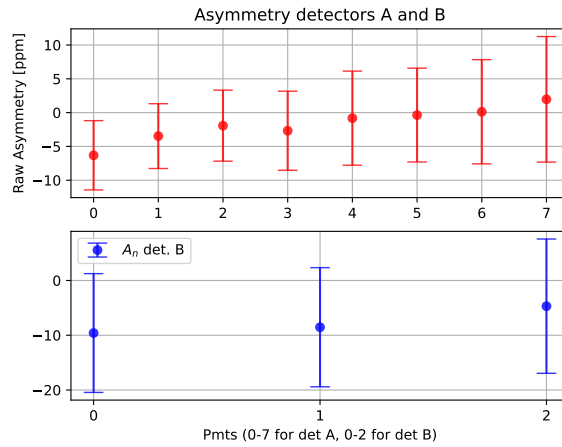


Figure 5.3: Raw-asymmetry computed for the block of runs with  $P = 0$ . Except for one PMT of detector A, all the values are compatible with 0 in  $1\sigma$ .

This plot unequivocally shows that all the asymmetries measured for each PMTs for both detector A and B are compatible with zero. It is therefore reasonably certain that such data should not be included in the main analysis.

Even if those data are not useful in reconstructing the final asymmetry, they are still useful to check the presence of systematic effects. Because we are reasonably sure that  $P = 0$  for these data, the presence of a small deviation from  $A = 0$  is a way to identify the presence of an offset. These data are treated likewise the other data with right polarization setting.

### 5.3.1 Fit with a linear model

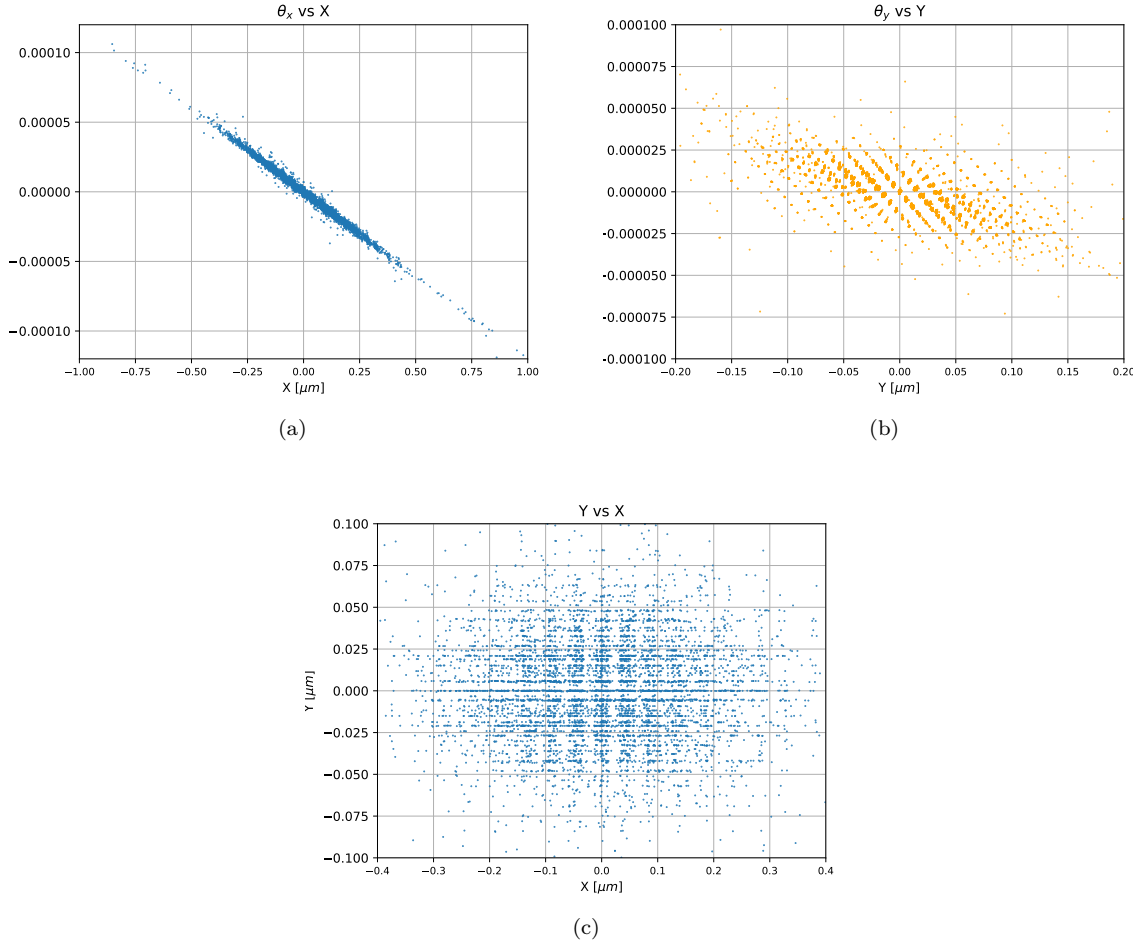
To retrieve the asymmetry  $A_n$  from the data, we assume a linear model where the asymmetries depend on the beam parameters, in the way we discussed before (5.2). The contributions due to variations of the beam within an events are described with 5 parameters, that are  $A_x, A_y, A_{\theta_x}, A_{\theta_y}, A_E$ . The data are analyzed both using python libraries, and with a fit program implemented in the framework of this thesis. To analyze the data with python, it is used the *curvefit* function implemented in the python library *scipy*. The fit program implements a well known algorithm used in linear regression: the ordinary least square algorithm (OLS). The OLS algorithm is basic algorithm, the easiest to implement and robust. It relies on few important hypothesis about the characteristics of the data. In principle we could handle all the analysis relying entirely on python. The decision to implements a fit program by ourself is due to the fact that in this way we interface directly to the analysis program, that is written in *c++* code. the assumption underlying linear regression is that there is a relation between the data of this type:

$$y = \vec{x} \cdot \vec{\beta} + \epsilon \quad (5.6)$$

$\vec{x}$  are the independent variables,  $\vec{\beta}$  are the parameters and  $\epsilon$  is a noise, that is supposed to be gaussian distributed (however, the robustness of the OLS algorithm let to relax this request). Another important assumption is that the linear variables are not correlated. This last request is particularly important, as related data cannot be processed with either of the two algorithms used. Before proceeding with the fit, it is necessary to verify this assumption. The first step so is to compute the correlation matrix for the beam parameters, we report in a table the values obtained:

•	X	Y	$\theta_x$	$\theta_y$	E
X	1	-0.019	-0.995	0.056	0.036
Y	-0.019	1	0.006	-0.647	0.005
$\theta_x$	-0.995	0.006	1	-0.005	-0.05
$\theta_y$	0.056	-0.647	-0.05	1	-0.003
E	0.036	0.005	-0.05	-0.003	1

It's immediate to observe that for  $(\theta_x, X); (\theta_y, Y)$  the values for the correlation are high compared to the other parameters.



The plots confirm the linear dependence between those parameters. With this evidence, it's clear that the have to modify the model to fit the data. We decided to include as linear independent variables only :  $I, X, Y, E$ .

Before proceeding with the fit, it's interesting to study how  $A_n$  evolves with the increase of the data. What we intend is to plot the averaged values  $\bar{A}_n$  as the number of data increases, where the average is made on all data collected from time  $t = 0$  up to time  $t = t_1$ .

These plots are useful to check that the asymmetries converge to a certain value, and that there are no steepy variations that could be related to the presence of remaining outliers. Besides this we observe that the sign of the asymmetries for the two detector are opposite, in agreement with what we expect from the kinematic. For a better visualization of the data, especially to observe the dependence of the asymmetry on the Beam parameters measured, it is useful to plot  $A$  versus each of the beam parameters. Unfortunately, the statistical error associated to the asymmetry is too high to appreciate whether there is a linear dependence in the data.

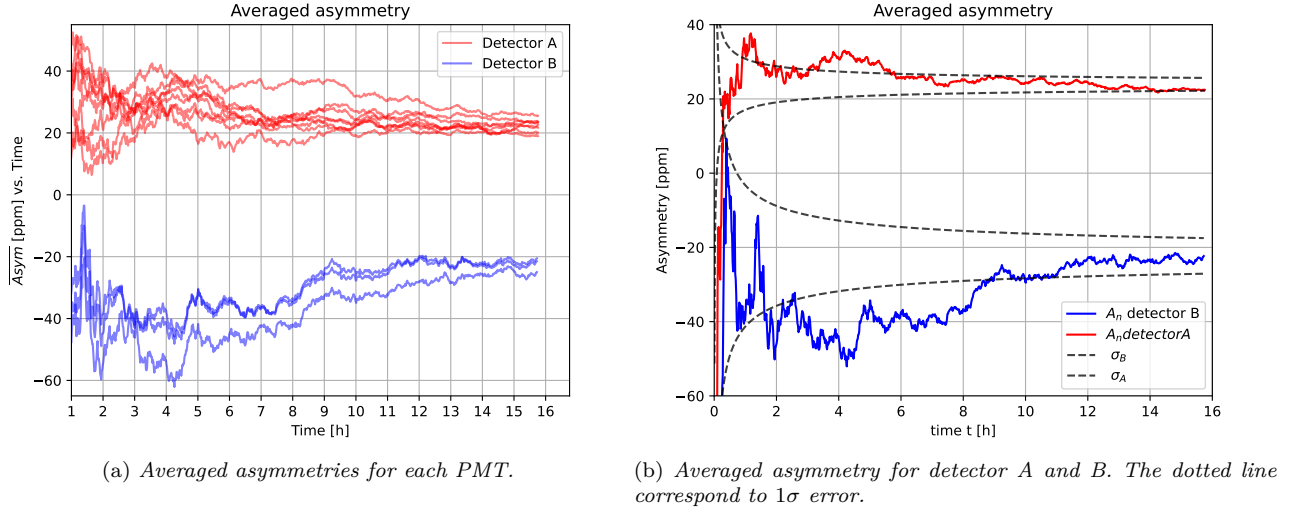


Figure 5.4: Plot of the Asymmetry versus time. The plot show the average over all the events collected from  $t = 0$  to  $t = t_1$ . Each line represents  $A_n$  measured for PMT (in blue detector B and in red detector A). The values are corrected for the beam polarization, multiplying by  $\frac{1}{p}$ . No further correction is applied.

detector A	X	Y	E
linear fit $\chi^2_{17}$	99	59	94
model $\chi^2_{16}$	76	55	78

For example here we plot  $A$  versus  $X$ .

We see large vertical band of points, and it's quite hard to identify a trend in the values. A different approach is to divide the  $X$  axis in small interval, like the procedure of binning, and average all the asymmetries that fall in the same interval. This reduce the dimensionality of the data, and let us to see if our assumption of the linearity is true. Each point represents the overall asymmetry for a particular interval of  $X$ ,  $Y$  and  $E$ .

The errors shown are computed with the same formula defined in 2.7:

$$\sigma_{Asym} = \frac{1}{\sqrt{2N_{A/B} \cdot n}}$$

We decided to analyze the data considering each beam parameter separately, too. Because we already delete the beam parameters with high correlations, this should not produce a bias. For the  $X$  and  $Y$  positions, Two model are used to fit the data. The first one is the linear model:

$$A = m \delta x + A_{phys} \quad (5.7)$$

For the second model, we decided to use the following polynomial:

$$A = c \delta x^5 + m \delta x + A_{phys} \quad (5.8)$$

For the energy monitor, we have:

$$A = c \delta E^3 + m \delta E + A_{phys} \quad (5.9)$$

This choice is due to the fact that we observe that  $A$  increases near the tails of the plot, the odd exponent is due to the fact that  $A$  has a different sign, positive for left and negative for right.

The values of the fit are reported in the plots. The  $\chi^2$  of the fit are reported here

The  $\chi^2$  values are higher than the expected and we observe that the values for the model 2 are lower than the ones of linear fit. This high values can be explained with two considerations: the first one is that this procedure of averaging the data based on  $x$  interval leads to the loss of information that can influence the fit, the second consideration is that we are ignoring the possible error in the determination of  $\delta x$ . Despite this, we observe that the for the  $\delta x$  and  $\delta y$  the values associated to  $A_{phys}$  are almost the same considering the first or the second model. For  $\delta E$  we see that  $A_n$  is slightly different. It was therefore chosen to use both the linear models:

$$A_{tot} = A_{phy} \cdot P + \delta_I + A_x \delta x + A_y \delta y + A_E \delta E \quad (5.10)$$

the result are reported in 6.2.

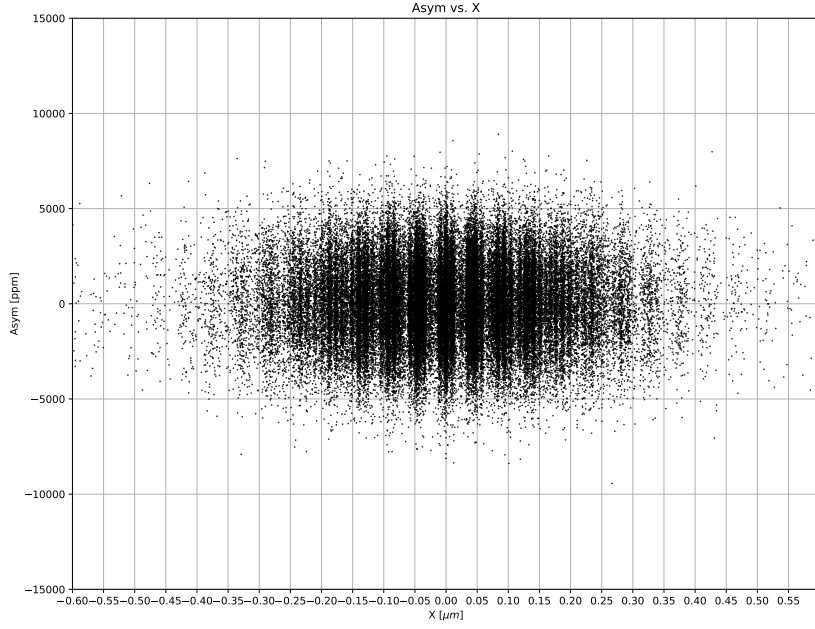


Figure 5.5: Measure of PMT A0 versus X beam position. The statistical uncertainties of the asymmetry doesn't let to recognize the presence of a linear dependence in the data.

## 5.4 False asymmetries

Until now the values for the false asymmetries were treated as the parameters of the fit. In this section we will investigate how we can obtain another different estimations, useful to check the validity of all the process of analysis of the data.

For  $\frac{dA}{dX}$  and  $\frac{dA}{dY}$ , we conceptually exploit the possibility of varying the position of the beam on the target, as we did during one of the calibration phases. Using the same *wobbler 16* we asked MAMI to slowly change the beam position on the X and Y monitor. The change in position has the effect to modify the rates for the two detector, and from them it's possible to extract estimate the two false asymmetries related to the beam position. Now we will see how the two quantities are related. From the plot .. we see that the counts are scaling linearly with the beam position, so we assume that the  $N$  are given by

$$N(x, \dots) = N_0 + m \cdot (x - x_0)$$

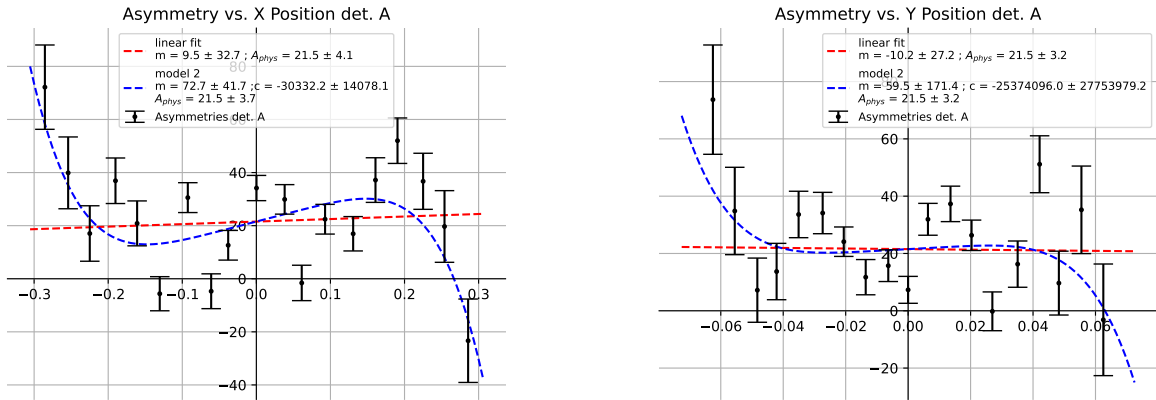
it is clear that the linear model can't be always good, at some point the electron will be deflected completely out of the detector, and so the counts will fall rapidly to zero. However, the magnets used to deflect the beam are producing small variation in the position, on the order of hundredths of a millimeters. Let's suppose that the beam position for two sub-events is  $x_1$  and  $x_2$ , we can calculate the asymmetry between the two event, taking care of the possible effects due to the different position. We write explicitly:

$$Asym = \frac{N(x_1) - N(x_2)}{N(x_1) + N(x_2)} = \frac{N_0 + m \cdot (x_1 - x_0) - N_0 - m \cdot (x_2 - x_0)}{N(x_1) + N(x_2)} = \frac{m}{2N_0 + m \cdot (x_1 + x_2) - 2mx_0} (x_1 - x_2) \quad (5.11)$$

In this equation three different parameters appear:  $N_0$  is the offset of the linear model,  $m$  is the angular coefficient, or the slope, and  $x_0$  is the initial position respect to we compute the position variation. The first two terms are obtained by a linear fit, while  $x_0$  is fixed conveniently.

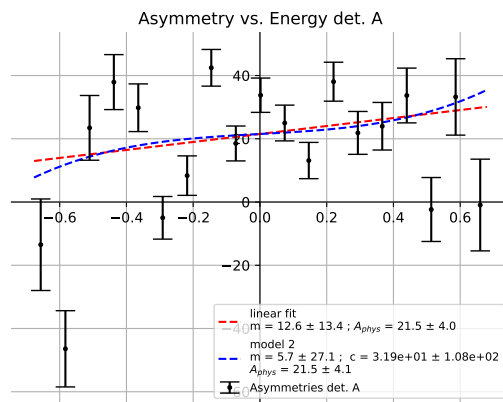
We can approximate the denominator deleting the term  $m \cdot (x_1 + x_2)$  which should be small compared to  $2N_0$ . We end with:

$$Asym = \frac{m}{2N_0 - 2mx_0} (x_1 - x_2) \quad (5.12)$$

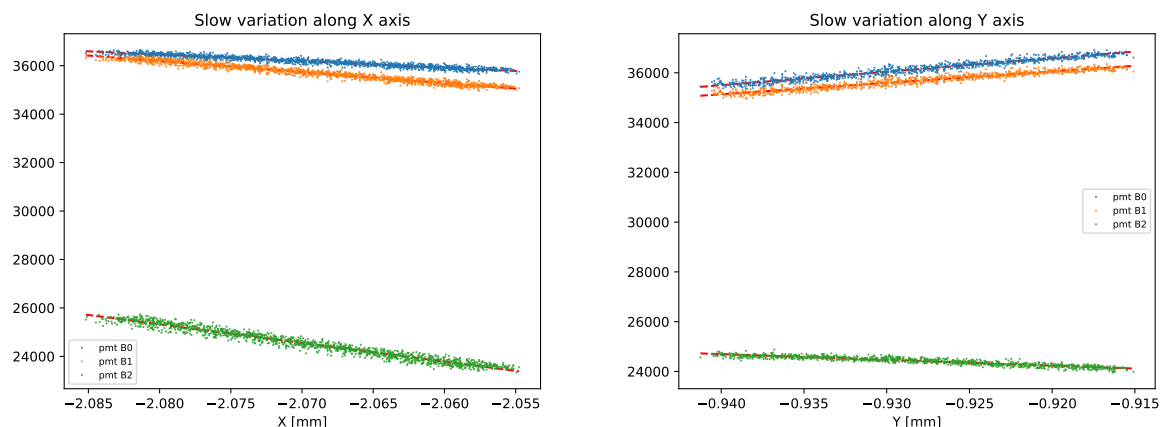


(a)  $A$  versus  $\delta x$ , the linear model is the red line, the second used to fit the data is a polynomial, represented in blue.

(b)



(c)



(a) Plot for slow variation in  $x$  direction for detector B.

(b) Plot for slow variation in  $x$  direction for detector B.

The term in front of  $(x_1 - x_2)$  can be compared to  $\frac{dA}{dX}$ .  $x_0$  is arbitrary and can be set to 0. For  $N_0$ , the offset, we substitute the averaged value counts of each PMT for the polarized beam acquisitions ( we remind that the rate are collected during each 20 ms time interval of each sub-event).

The data are reported in the table below:

PMT	Detector A	Detector B
PMT 0	84718	18925
PMT 1	96882	18815
PMT 2	80604	14807
PMT 3	65053	
PMT 4	45943	
PMT 5	46248	
PMT 6	37452	
PMT 7	25808	

We report the values obtained with this new method ...

We can investigate also the asymmetries related to the beam energy. For this one we can exploit the theoretical expression for the Mott cross-section, taking the derivative ...

We can investigate the Current asymmetries, because we have the auto-calibration procedure, so from the scale factor we can check if the current asymmetri is compatible with 1 as assumed or not.

## 5.5 ??Bootstrap??

# Chapter 6

## Result

In this chapter we report the result obtained for the data-analysis. First we report the averaged asymmetries with and without subtracting the pmt offset. From the asymmetry results, we can compute the factor  $c$  as the ratio between the final asymmetries with and without subtracting the offset. The values can be directly confronted with the ones defined in 4.3.6. We see a good agreement. All the values are in reported in ppm (part-per-million).

PMT	Average	$\sigma$	PMT	Average	$\sigma$	PMT	$c$
B0	-19.92	7.7	B0	-20.61	8	B0	0.97
B1	-19	7.8	B1	-19.69	8	B1	0.96
B2	-23.42	8.7	B2	-24.13	9	B2	0.97
A0	18.8	3.7	A0	24.55	4.2	A0	0.77
A1	16.05	3.4	A1	22.54	4.1	A1	0.71
A2	18.45	3.7	A2	24.37	4.3	A2	0.76
A3	19	4.2	A3	23.49	4.7	A3	0.81
A4	20.84	5	A4	24.21	5.4	A4	0.86
A5	22.83	4.9	A5	26.39	5.3	A5	0.87
A6	17.49	5.5	A6	19.82	5.9	A6	0.88
A7	19.24	6.6	A7	20.97	6.9	A7	0.92

(a) Asymmetries, with offset  
not subtracted.

(b) Asymmetries with offsets  
subtracted

(c)  $c$  factor, as de-  
fined in 4.7

Table 6.1: Averaged asymmetries over all the events. The values are corrected subtracting  $\bar{A}_I$  and considering the effective polarization  $p$  of the beam

The asymmetries are shown with the errors in the following plot. The error are obtained with the formula:

$$\sigma = \sqrt{\frac{1}{2N \cdot n}}$$

To Obtain a final asymmetry for detector A and B, the asymmetries for each plot are averaged using the formula:

$$\bar{A}_n = \sum_{i=0}^{n_{PMT}} \frac{w_i A_i}{\sum_{i=0}^{n_{PMT}} w_i} \quad (6.1)$$

This is a weighted mean, and  $w_i = \frac{1}{\sigma_i^2}$ . This formula is applied to take care of the different statistical error for different pmts.

The overall results for the two detectors are:

- Asymmetry for detector A,  $A_A = 23.1 \pm 1.6$  ppm.
- Asymmetry for detector B,  $A_B = -22.7 \pm 4.7$  ppm.

### 6.1 Best fit

The result obtained from the linear fit of the asymmetries versus the beam parameters are reported here, together with the false asymmetry values. In this case the model is quite simple: only  $X$ ,  $Y$ ,  $E$  are the beam parameters:

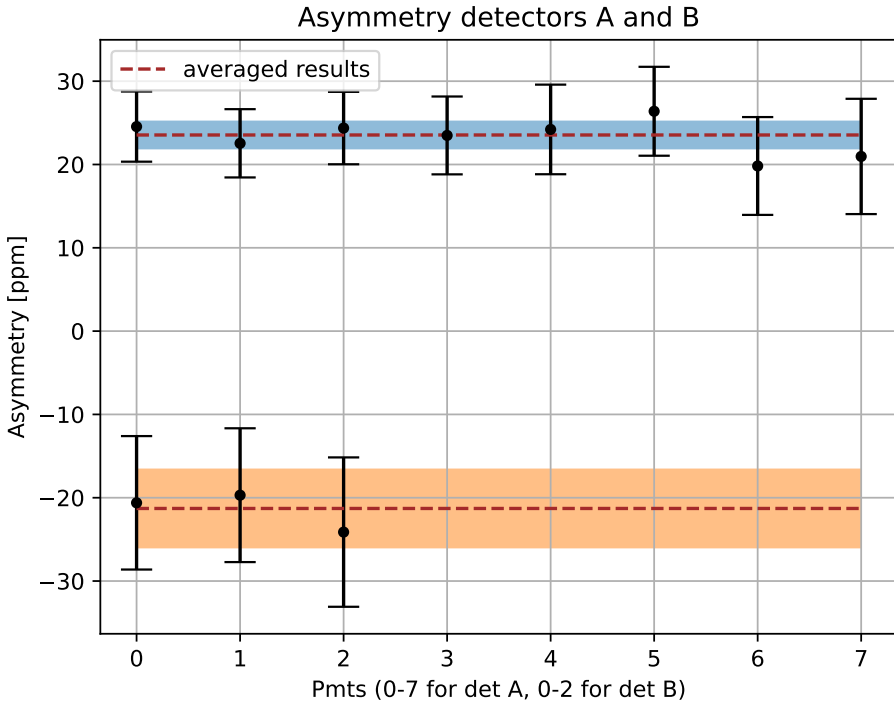


Figure 6.1: Plot of the asymmetries ordered by the pmt label, the result are the average event per event, corrected by the beam asymmetry current and for the polarization  $p$  percentage.

The result for detector A:

PMT	$A_n$	$A_x$	$A_y$	$A_e$	$\chi^2_{reduced}$
A0	$24 \pm 4$	$53 \pm 27.4$	$-45 \pm 135$	$11.8 \pm 12$	$1.000 \pm 0.002$
A1	$23 \pm 4$	$-4.9 \pm 26.3$	$-122 \pm 130$	$23.3 \pm 11$	$1.001 \pm 0.002$
A2	$23 \pm 4$	$-26 \pm 27.2$	$-61 \pm 134$	$12.4 \pm 12$	$1.000 \pm 0.002$
A3	$23 \pm 5$	$0 \pm 28.8$	$-218 \pm 142$	$2.9 \pm 12$	$0.999 \pm 0.002$
A4	$24 \pm 5$	$36 \pm 30.7$	$-122 \pm 151$	$7.6 \pm 12$	$1.000 \pm 0.002$
A5	$27 \pm 5$	$17 \pm 30.9$	$161 \pm 152$	$-2.9 \pm 13$	$1.001 \pm 0.002$
A6	$20 \pm 5$	$-7 \pm 33.3$	$104 \pm 164$	$2.5 \pm 14$	$1.000 \pm 0.002$
A7	$20 \pm 6$	$-7.8 \pm 37.5$	$41 \pm 185$	$19.8 \pm 16$	$1.001 \pm 0.002$

Table 6.2: fit result with the linear model, for detector A.

the result for detector B:

PMT	An	Bx	By	Be	$\chi^2_{reduced}$
B0	$-22 \pm 8$	$-87 \pm 40$	$-243 \pm 186$	$21 \pm 18$	$1.000 \pm 0.002$
B1	$-21 \pm 8$	$-92 \pm 40$	$-167 \pm 187$	$14 \pm 18$	$1.000 \pm 0.002$
B2	$-26 \pm 9$	$-92 \pm 46$	$-383 \pm 210$	$-24 \pm 20$	$1.000 \pm 0.002$

Table 6.3: fit result with the linear model, for detector B.

The overall result for  $A_n$  for both the two detectors:

DETECTOR	An
A	$22.8 \text{ pm } 1.7$
B	$-22 \pm 5$

Table 6.4: Overall result for detector A and B.

## **Chapter 7**

# **Conclusion and outlook**

# Appendices

## **Appendix A**

### **Some Appendix**

The contents...

# Bibliography

- [1] Single and multichannel, synchronous voltage-to-frequency converters, ad7741. *Analog Devices*.
- [2] Strahldiagnostik und analyse der optischen eigenschaften des strahlführungssystems von mami. *Diplomarbeit*, 2004.
- [3] A. Esser, M. Thiel, P. Achenbach, K. Aulenbacher, S. Baunack, J. Beričić, D. Bosnar, L. Correa, M. Dehn, M. O. Distler, H. Fonvieille, I. Friščić, M. Gorchtein, S. Heidrich, P. Herrmann, M. Hoek, S. Kegel, Y. Kohl, T. Kolar, H.-J. Kreidel, F. E. Maas, H. Merkel, M. Mihovilović, J. Müller, U. Müller, F. Nillius, C. Palatchi, K. D. Paschke, J. Pochodzalla, B. S. Schlimme, M. Schoth, F. Schulz, S. Širca, B. Spruck, S. Štajner, V. Tioukine, A. Tyukin, A. Weber, and C. Sfienti. First measurement of the  $Q^2$  dependence of the beam-normal single spin asymmetry for elastic scattering off carbon. *Phys. Rev. Lett.*, 121:022503, Jul 2018.
- [4] M. Gorchtein and C. J. Horowitz. Analyzing power in elastic scattering of electrons off a spin-0 target. *Physical Review C*, 77(4), apr 2008.
- [5] B.S. Schlimme, P. Achenbach, K. Aulenbacher, S. Baunack, D. Bender, J. Beričić, D. Bosnar, L. Correa, M. Dehn, M.O. Distler, A. Esser, H. Fonvieille, I. Friščić, B. Gutheil, P. Herrmann, M. Hoek, S. Kegel, Y. Kohl, T. Kolar, H.-J. Kreidel, F. Maas, H. Merkel, M. Mihovilović, J. Müller, U. Müller, F. Nillius, A. Nuck, J. Pochodzalla, M. Schoth, F. Schulz, C. Sfienti, S. Širca, B. Spruck, S. Štajner, M. Thiel, V. Tioukine, A. Tyukin, and A. Weber. Vertical beam polarization at MAMI. *Nuclear Instruments and Methods in Physics Research Section A: Accelerators, Spectrometers, Detectors and Associated Equipment*, 850:54–60, apr 2017.